Fuel Processing Technology 235 (2022) 107348

Contents lists available at ScienceDirect

Fuel Processing Technology

journal homepage: www.elsevier.com/locate/fuproc

Understanding the mechanism of two-step, pyrolysis-alkali chemical activation of fibrous biomass for the production of activated carbon fibre matting

James M. Illingworth, Brian Rand, Paul T. Williams *

School of Chemical & Process Engineering, University of Leeds, Leeds LS2 9JT, UK

ARTICLE INFO

Keywords:
Biomass
Chemical activation
Activated carbons
Mechanisms

ABSTRACT

Pyrolysis of fibrous biomass followed by alkali (KOH and K_2CO_3) chemical activation of the pyrolysis char for the production of activated carbon fibre matting material has been investigated. For KOH, activation initially involved the melting of the KOH and reaction with the disorganised/volatile material of the char, producing hydrogen gas and K_2CO_3 and further developing the existing pore structure of the char. At higher temperatures (>700 °C), pore widening occurs due to physical activation with less reaction of the alkali molten phase with the char. Metallic potassium or other potassium species may also contribute to the pore widening process. Chemical activation with K_2CO_3 occurs at higher temperatures (>600 °C) and is controlled by the decomposition of K_2CO_3 to K_2O and CO_2. The development of surface area and porosity occurs through reaction of the pyrolysis char with K_2O and CO_2. The production of CO_2, enhances the physical activation of the pyrolysis char, leading to widening of pores. KOH activation results in the development of micropores at low temperatures, followed by pore widening at higher temperatures. For K_2CO_3 activation, pore creation and pore widening occur simultaneously at higher temperature, resulting in a lower micropore volume and a wider pore size distribution.

1. Introduction

Activated carbons possess high surface area, a well developed porosity with high adsorption characteristics and are a widely used material throughout industry particularly as adsorbents for control of air and water pollution with a global market of several billion dollars [1]. Activated carbons have been produced from a variety of materials including coal, petroleum residue and biomass. In particular, agricultural biomass wastes have been extensively investigated for the production of activated carbons since they represent an extremely large and readily available resource [1–5]. For example, Yahya et al. [1] have reviewed different biomass types used for activated carbon production [1], Ukanwa et al., [2] and Gayathiri et al. [5] reviewed the process variables for activated carbon production and Zhang et al. [4] reviewed the synthesis, formation mechanism and applications of activated carbons. In addition, production of activated carbons from waste biomass would be more environmentally sustainable and produces a higher value product to offset the costs of waste management. Activated carbons have been produced from a wide range of agricultural waste feedstocks, including corn biomass [6], cotton stalks [7], bamboo [8], date palm stones [9], coconut shells [10], wheat straw [11] etc.

The production of activated carbons from waste biomass involves physical or chemical activation. Physical activation involves pyrolysis of the biomass to produce a char followed by activation with steam or carbon dioxide at high temperature (700–1000 °C). Chemical activation involves treatment of the raw biomass by impregnation with a chemical activating agent such as zinc chloride, phosphoric acid, potassium hydroxide, potassium carbonate or sodium hydroxide followed by carbonisation at temperatures typically between 400 and 800 °C. Alternatively a two-step process is used for chemical activation, where the biomass material is firstly pyrolysed to produce a char followed by impregnation of the char with the chemical activation agent and finally the impregnated char is activated at high temperature to produce the activated carbon [2]. The two-step process has the advantages of producing an enhanced carbon content and the first pyrolysis stage produces an initial porosity which is further developed with the chemical activation processing.

One particular type of biomass agricultural waste that has received attention is biomass fibrous waste with the intention that a fibrous activated carbon is produced and applied in a wide range of applications

* Corresponding author.
E-mail address: p.t.williams@leeds.ac.uk (P.T. Williams).

https://doi.org/10.1016/j.fuproc.2022.107348
Received 31 March 2022; Received in revised form 26 May 2022; Accepted 1 June 2022
Available online 13 June 2022

such as supercapacitor manufacture [12,13], organic medical waste pollutants removal from waste waters [14] dye removal [15,16] and for SO_2 gas cleaning [17]. Activated carbon fibres have exceptional characteristics because of their fibrous structure, high surface area with high microporosity, high volumetric capacity, high packing density and fast adsorption kinetics [18]. A further advantage of using waste fibrous biomass as the precursor for the production of activated carbon is that the fibrous nature of the biomass allows the fibres to be processed to produce a fabric-like matting material and subsequently an activated carbon fibre material. Using textile-processing techniques such non-woven technology, the fibrous biomass can be manufactured into a fabric like, non-woven matting material which can subsequently be pyrolyzed and activated to produce a non-woven activated carbon fibre matting [19–21]. Such a product can then be easily and directly used in pollution abatement applications, rather than requiring further processing such as granulation of the carbon, cartridge packing or attachment to a support material as required for traditional powdered activated carbon.

The mechanism for the production of activated carbon fibres derived from fibrous biomass waste through alkali chemical activation is very complicated [22]. In addition, the mechanism for the specific process of two-step pyrolysis of fibrous biomass waste followed by chemical activation using alkali-salt impregnation of the char and subsequent carbonation at high temperature is also not well described.

In this paper, a detailed investigation of the chemical activation process of fibrous biomass flax char using different alkali metal salts for the production of fibrous activated carbon matting has been undertaken. The time/temperature profiles of gas evolution was linked to the surface area and porosity properties of the product activated carbon. The aim of the work was to describe the process and to develop an understanding of the formation mechanism for the production of the activated carbon.

2. Materials and methods

2.1. Materials

The precursor biomass material used to produce the activated carbons was low-grade flax fibre obtained from British Fibres Limited, UK. The fibrous material contained ‘shive’ material from the ‘scutching’ process, where the fibres were cleaned following the retting stage of fibre separation. The ‘as-received’ raw fibre was converted into a non-woven fabric material involving a process where the fibres are incorporated into a carded web using a technique known as ‘dry laid carding’. This method employs rotating cylinders covered in wires or teeth that arrange the fibres into parallel arrays. The position of the cards can then be positioned to alter the direction in which the fibres are laid, thus providing a greater cross directional strength within the fabric material. For this work, the material was manufactured at a uniform thickness of 8 mm. The fabric produced is then subjected to needlepunch bonding. In this process, barbed needles are punched through the fabric, hooking tufts of fibre and tangling them together, which enhances the strength and stability of the non-woven fabric. Finally, the material is rolled between two heated cylinders, in a process is known as ‘calendar bonding’, where heat (75 °C) and pressure (1 t) causes the fibres to fuse, again adding to the structural stability of the final produced fabric material.

The product non-woven biomass fabric material has characteristics of strength combined with flexibility and make an ideal filter-media as a result of their random, dispersed fibrous structure [23]. Therefore, the production of an activated carbon material in the non-woven form has the potential to be used directly in pollution abatement applications without the need for expensive containment or further processing [17].

The elemental analysis (C, H, N, S, O) of the flax fibre, char and activated carbon samples was carried out using an elemental analyser (CE Instruments Flash EA 1112). The results showed a carbon content of 43.5 wt%, hydrogen 6.7 wt%, nitrogen 1.7 wt% and oxygen 48.5 wt% (by difference), no sulphur was detected. Proximate analysis of the raw flax fibre was determined according BS1016 part 3, and showed 7.5 wt% moisture content, 75.6 wt% volatiles, 15.2 wt% fixed carbon and 1.7 wt % ash content.

2.2. Production of pyrolysis chars

A laboratory scale fixed-bed batch reactor was used for the pyrolysis of the non-woven flax material to produce a char for later chemical activation (Fig. 2). The pyrolysis reactor was constructed of stainless steel and was 200 mm in length with an internal diameter of 65 mm, enabling the pyrolysis of up to 60 g of biomass material. The reactor was heated externally by an electrically heated furnace and fully controllable with thermocouples used to monitor temperature. The reactor was continually purged with nitrogen. Liquid products were condensed in a series of dry-ice cooled condensers, followed by transfer of product gases to a Tedlar™ gas sample bag. Strips of the non-woven biomass material of mass ~ 30 g were used for the pyrolysis procedure (approximate dimensions - 300 mm × 100 mm) and was rolled and packed into the pyrolysis reactor. To maximise the yield of char, slow pyrolysis conditions were used, consisting of heating the reactor from ambient temperature to a final pyrolysis temperature of 800 °C at a heating rate of 2 °C min^{-1}, and held at 800 °C for a further 60 min. Table 1 shows the reproducibility of the char production process, showing a mean char production of 22.17 wt% of biomass. The product liquid bio-oil comprised ~55 wt% of the total product yield and has been reported to be chemically complex, with high oxygen and water content, acidic properties and tendency to polymerise. Therefore, for the development of the overall process, further processing of the bio-oil would be required to produce a higher quality liquid fuel product or for use as petroleum refinery feedstock. The yield of product gas was ~23 wt% and has been shown to be composed of mainly CO, CO_2, H_2 and CH_4, with potential for use as a low grade process fuel to provide the energy requirements for the pyrolysis process. Fig. 1(b) shows the non-woven biomass flax material pyrolysis char produced at a pyrolysis temperature of 800 °C.

2.3. Production of activated carbons by chemical activation

The pyrolysis char was converted to activated carbon using a chemical activation process, where the char was impregnated with alkali metal salts and activated at high temperature, followed by washing of the product activated carbon to remove the activating chemicals. The same reactor as used for pyrolysis and described above was used for the activation process (Fig. 2). The non-woven biomass flax pyrolysis char material was dried overnight at 110 °C and then ~2.00 g sample quantities of the char was cut from the material and mixed with 50 ml of deionised water containing the desired mass of activating chemical to achieve a known impregnation ratio. The sample was then evaporated to dryness at 80 °C before thorough drying at 110 °C for 24 h. The impregnated chars were then heated at 5 °C min^{-1} to the activation temperature of 800 °C under nitrogen flow. Hold times at the final temperature were varied between 0 and 3 h. Following activation, the

Table 1
Reproducibility of the char production process.

Pyrolysis temp (°C)	Initial mass (g)	Char (wt %)	Liquid (wt %)	Gas* (wt %)
800	33.33	22.33	55.43	22.24
800	34.93	21.96	54.65	23.39
800	34.15	22.17	54.87	22.96
800	35.49	21.97	55.65	22.38
800	33.91	22.42	55.03	22.55
Mean		22.17	55.12	22.70
Standard Deviation		0.208	0.409	0.469
Std. Dev (% mean)		0.936	0.741	2.07

* By difference.

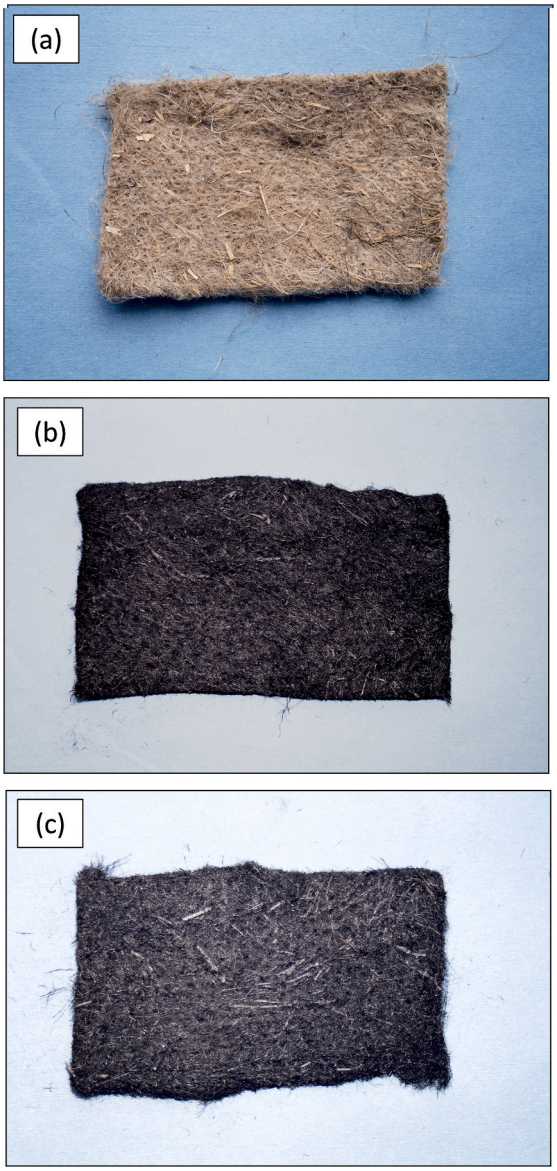

Fig. 1. (a) Non-woven biomass flax fibre precursor matting material; (b) Pyrolysis char non-woven matting produced at a pyrolysis temperature of 800 °C; (c) Non-woven activated carbon produced at 1:1 ratio of KOH from the pyrolysis char produced at 800 °C.

samples were cooled overnight under nitrogen and then washed sequentially with hot, cold and then deionised water until the washing water reached a stable pH of 7 to 7.5. The samples were then dried at 110 °C for 24 h, weighed and stored in a desiccator in sealed vials. An example of the activated carbon fibrous biomass material is shown in Fig. 1(c) for the activated carbon produced with a 1:1 ratio of KOH.

An estimate of the amount of activating chemical recovered during the washing process was made according to Eq. (1):

$$CR\ (wt\%) = (C_2/C_1) \times 100 \quad (1)$$

Where: CR = chemical recovery (wt%).

C_2 = mass of chemical removed during washing process (g).

C_1 = mass of chemical impregnated (g).

The yield of the activation procedure was calculated according to Eq. (2):

$$Yield\ (\%) = (W_2/W_1) \times 100 \quad (2)$$

Where: W_1 = Initial dry mass of char (g).

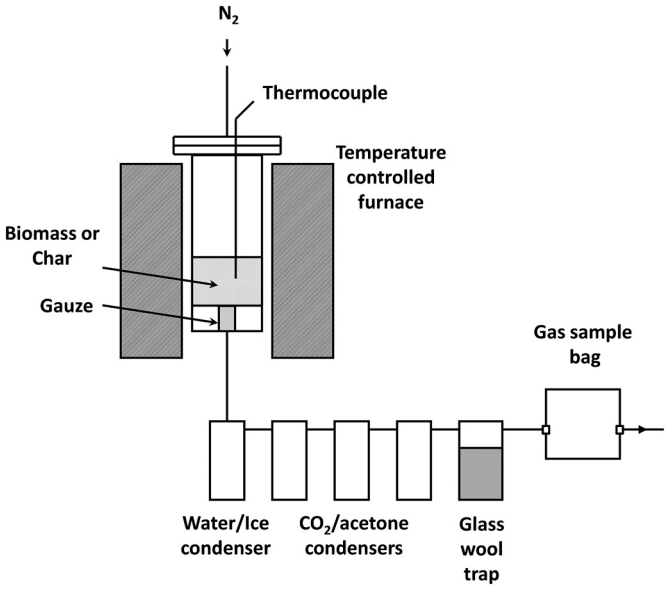

Fig. 2. Schematic diagram of the pyrolysis and activation reactor.

W_2 = Dry mass of carbon following activation and washing (g).

The repeatability of the chemical activation procedure was assessed. An 800 °C flax char sample was impregnated with a 1:1 ratio (by weight) of KOH and activated at 800 °C for 2 h. The activation was repeated three times. Repeatability was assessed according to product yield, chemical recovery and porous texture data determined by gas adsorption. The resulting data is presented in Table 2 and shows good repeatability, particularly regarding the yield of the process and the porous texture of the resulting carbons. The chemical recovery data are more variable but still show a relative standard deviation of below 10%.

In addition, limited work was carried out on the physical activation of the biomass flax pyrolysis chars using carbon dioxide as the activating agent to produce activated carbons for comparison with the chemically activated carbons. The pyrolysis chars (~2.00 g) were physically activated using the same activation reactor (Fig. 2) which was heated at 5 °C min^{-1} to a final activation temperature of 825 °C under N_2 then switched to CO_2 for activation, for the desired period of activation (from 1 to 6 h). At the end of the activation period, the carbon product was cooled under nitrogen then dried at 110 °C and stored in a desiccator in sealed vials.

Table 2
Reproducibility of the chemical activation process.

	Yield [wt%]	Chemical recovery [wt%]	A_{BET} [m^2/g]	V_{MIC} DR-N_2 [cm^3/g]	V_{MIC} DR-CO2 [cm^3/g]	V_{MES} [cm^3/g]
Experiment 1	80	51	1086	0.423	0.407	0.119
Experiment 2	79	56	1070	0.414	0.411	0.130
Experiment 3	77	48	1051	0.404	0.401	0.125
Mean	78.67	51.67	1069	0.414	0.406	0.125
Standard Dev^n	1.53	4.04	17.52	0.01	0.01	0.006
Std.Dev^n (% mean)	1.94	7.82	1.64	2.30	1.24	4.42

* A_{BET} = BET surface area; V_{MIC} = micropore volume; V_{MES} = mesopore volume.

2.4. Gas analysis

The product gases collected in the gas sample bag from the chemical activation of the flax biomass pyrolysis char were analysed by packed column gas chromatography. In addition, gas composition was determined as a function of time and furnace temperature, where gas samples were taken from the outlet of the reactor in gas syringes at 25 °C (5 min) intervals. The samples were then analysed by gas chromatography. The gas samples were analysed off-line by three separate packed column gas chromatographs (i) N_2, O_2, H_2 and CO: Pye Unicam series 204 chromatograph, fitted with a 1.8 m × 6 mm stainless steel column. The column was packed with a 5 Å molecular sieve. The carrier gas was argon with a constant flow rate of 24cm^3/min. The outflow of gases was monitored by a thermal conductivity detector. The injector, analytical column and detector were all maintained at 100 °C; (ii) CO_2: Gow Mac Spectra, fitted with a 1.8 m × 6 mm stainless steel column maintained at 105 °C. The column was packed with silica gel (100–120 mesh). The carrier gas was helium at a flow rate of 28cm^3/min. The concentration of CO_2 at the column exit was determined by a thermal conductivity detector. The injector, column and detector were all held at 105 °C; (iii) Hydrocarbons: Pye Unicam GCD, fitted with a 2.2 m × 6 mm glass column maintained at 35 °C. n-Octane Porasil 80–100 mesh was the column packing. The carrier gas was nitrogen at a slow rate of 28cm^3/min. The outflow of gases was monitored with a flame ionisation detector.

2.5. Char and activated carbon characterisation

The pore structure of the chars and activated carbons was characterised by gas adsorption using a Quantachrome Corp. Autosorb 1-C Instrument. The Autosorb 1-C operates by measuring the quantity of gas adsorbed onto or desorbed from a solid surface at some equilibrium vapour pressure by the static volumetric method. The instrument has the capability of measuring adsorbed or desorbed volumes of gas at relative pressures in the range 1×10^{-7} up to saturation pressure. Adsorption isotherms of nitrogen at 77 K were determined over a range of relative pressures from 1×10^{-6} up to 0.995. The desorption branch of the isotherm was measured down to a partial pressure of 0.025. The measurement of the isotherm over such a large range of relative pressure allows characterisation of the whole range of pore size classifications from micropores through to macropores. In addition, adsorption isotherms for CO_2 were produced over the relative pressure range 1×10^{-6} up to 0.03. Isotherms of carbon dioxide at 273 K allow a more accurate assessment of the narrowest micropores. Although the critical molecular dimensions of both gases are similar, the CO_2 molecule has far greater kinetic energy at 273 K than N_2 at 77 K, thus facilitating entry to very fine pores of molecular dimensions. The isotherms produced were analysed to determine the surface area, pore volumes and pore size distributions of the chars and activated carbons. Surface area was determined by the BET method and pore size distributions by density functional theory (DFT).

The true density of the activated carbons was determined by helium pychnometry using a Micromeritics Accupyc 1330 instrument. Samples were dried at 11 0 °C for 24 h prior to the helium density measurements. Sample weights were determined to an accuracy of 0.0001 g using a Sartorius 2001 MP2 analytical balance.

3. Results and discussion

3.1. Gases produced during chemical activation

The product gases produced during the chemical activation of the biomass flax pyrolysis chars with alkali metal salts involved initial experiments to determine the gaseous species released during the activation procedure. The chemical activation procedure was repeated three times using 1.00 g of pyrolysis char impregnated with a 1:1 ratio of KOH and heated at 5 °C min^{-1} to 800 °C and held at 800 °C for 2 h. Table 3 shows the total mass of gases evolved during the activation process. The main product gases evolved were hydrogen, carbon monoxide and carbon dioxide. No hydrocarbon gases were detected from the biomass flax char activation process. The results show that the total mass of evolved gases from the activation to be far higher than the total weight loss of the char, suggesting that the alkali metal salt and the char react to produce gaseous products during activation.

In addition, the evolution of the main product gases (H_2, CO and CO_2) was followed throughout the activation procedure in relation to time/activation temperature for activating chemicals KOH and K_2CO_3. A 1.00 g sample of biomass flax pyrolysis char was impregnated with a 1:1 ratio for KOH or 1.23:1 for K_2CO_3; for a given mass of alkali carbonate and hydroxide. To ensure the metal content remained identical to the hydroxide impregnated samples, the quantity of carbonate used was adjusted accordingly. The evolved gas samples during the activation process were withdrawn from the exit gas outflow at temperature intervals of 25 °C (at 5 mins timed intervals) throughout the activation process and were then analysed by gas chromatography. The gas evolution profiles are shown in Fig. 3. The results show that the evolution of the product gases becomes significant at an activation temperature of ~550 °C with the peak for CO and H_2 occurring together at 775 °C, whereas the peak for CO_2 production occurs slightly earlier at 700 °C. The gas evolution profile for the char activation with K_2CO_3 shows a close similarity for the two activating alkali chemicals.

The total quantities of the gases evolved were calculated (Table 4) and close agreement was observed between the two activating chemicals, suggesting that the chemical activation process is very similar for the KOH and K_2CO_3. KOH readily absorbs CO_2 from the atmosphere and undergo carbonation to produce K_2CO_3; (Reaction 1)

$$2KOH + CO_2 \rightarrow K_2CO_3 + H_2O \quad \text{(Reaction 1)}$$

It may therefore be suggested that the method of impregnation of KOH employed in the current work may have resulted in extensive conversion to the carbonate. Due to the morphology of the non-woven fibrous precursor, the impregnation procedure results in the formation of a fine layer of KOH over the char surface. Thereby, considerable exposure to CO_2 during the drying process would facilitate the carbonation of the KOH. To test this, 1.00 g of pyrolysis char was impregnated with KOH (1:1 ratio) but the drying time was reduced from 24 h to 4 h and carried out in a vacuum oven to reduce reaction between the KOH and CO_2 from the atmosphere. The sample was then activated and gas samples taken as before at 25 °C intervals and analysed by gas chromatography. The results of the evolved gas composition in relation to the time/temperature of activation are shown in Fig. 4 and the total gases evolved are shown in Table 4 (vac). A substantial increase (36%) in total hydrogen production was observed for the vacuum dried char KOH impregnation sample with evolution beginning far earlier than with the normal air dried sample. The release of hydrogen begins at a temperature of around 300 °C, peaks at 525 °C and then declines before rising again at 625-650 °C with a second peak at a temperature of 775 °C. The first peak (temperature, 525 °C) is absent for the 24 h air dried samples whereas the second peak corresponds with the hydrogen

Table 3
Total mass of gases evolved during the chemical activation process.

Gas species	Mass produced (mg)		
	Experiment 1	Experiment 2	Experiment 3
Hydrogen	13.2	13.1	11.3
Carbon monoxide	488	476	484
Carbon dioxide	147	139	129
Total gases	648	628	624
Total C released	249	242	242
Char weight loss	200	195	210
Chem weight loss	410	430	390

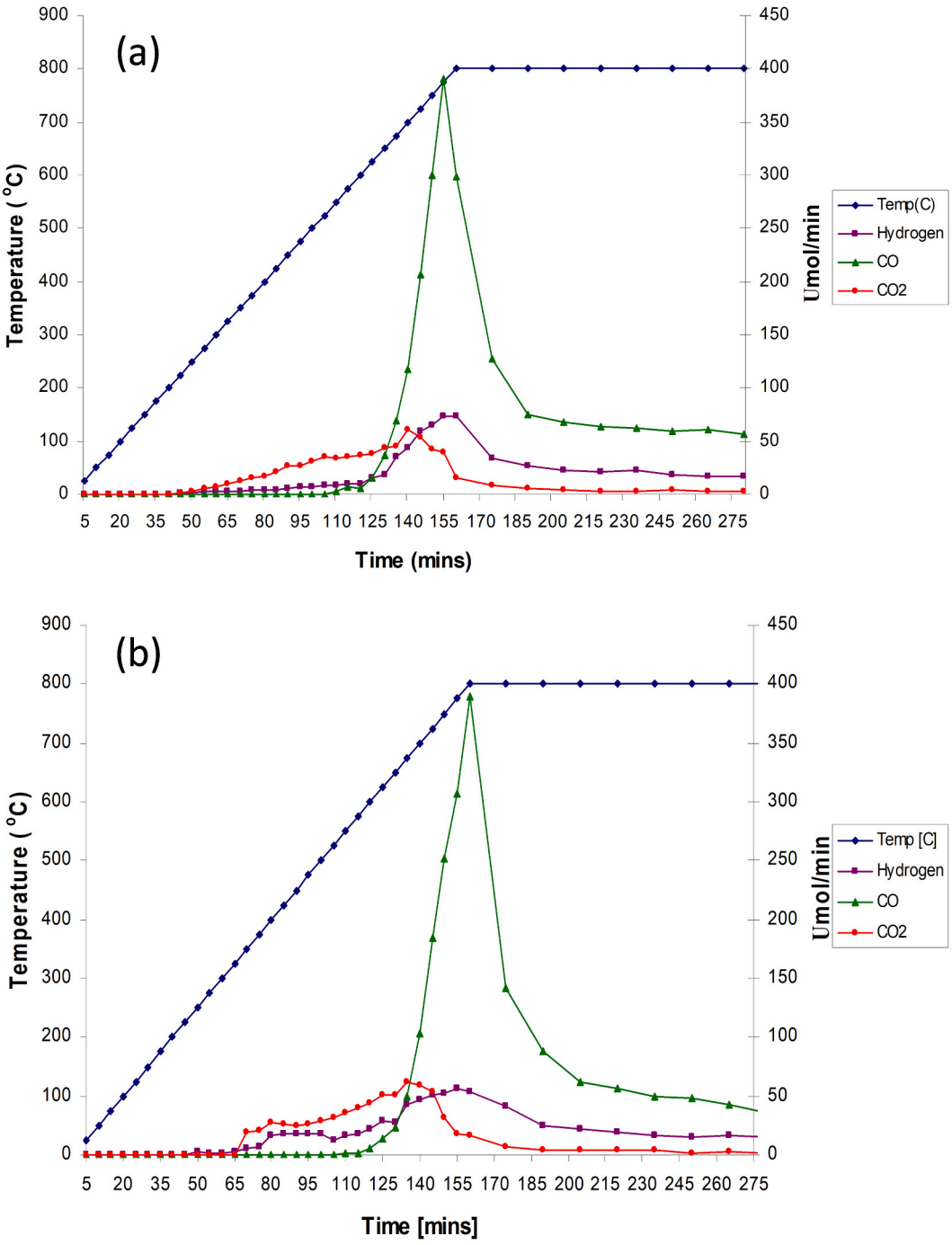

Fig. 3. Product gas evolution in relation to time/temperature for pyrolysis char (produced at pyrolysis temperature 800 °C) chemical activation (a) for KOH chemical activation agent: char ratio of 1:1 (b) for K_2CO_3 chemical activation agent: char ratio of 1.23:1.

Table 4
Evolution of product gases during chemical activation.

		Gases evolved (mg)		
Flax Char	Act. agent	CO	CO_2	H_2
800 °C	–	65	52	5.2
800 °C	KOH	473	169	11
800 °C	K_2CO_3	454	168	11
800 °C	KOH (vac)*	595	67	15

* (vac); 4 h drying under vacuum.

release for both (KOH and K_2CO_3) air dried samples (Fig. 3). The total evolution of CO_2 is reduced considerably in comparison to the air dried samples, with production commencing later and also peaking slightly later. This could be due to reduced CO_2 production or the KOH may be reacting with CO_2 in the reactor and converting to K_2CO_3. For CO, the shape of the peak is very similar but an overall increase in production is observed.

3.2. Surface area and porosity characteristics of the alkali chemically activated carbons

The surface area and porosity characteristics of the activated carbons

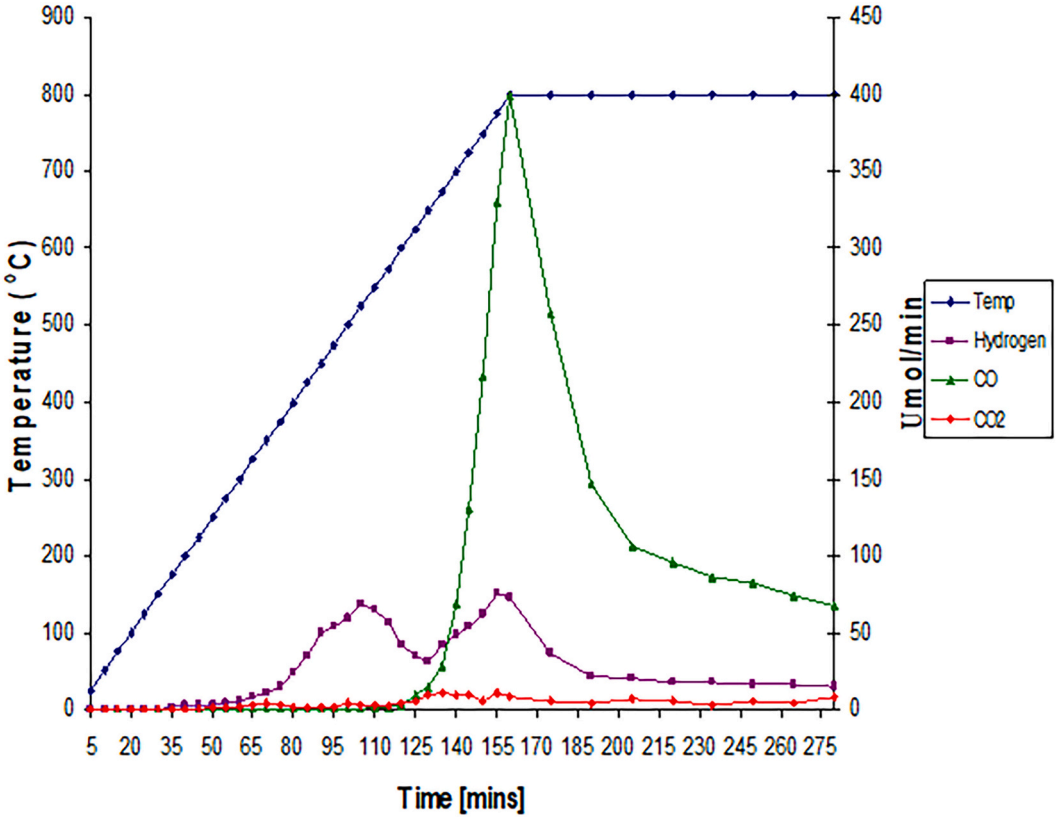

Fig. 4. Product gas evolution in relation to time/temperature for pyrolysis char (produced at pyrolysis temperature 800 °C) chemical activation with KOH (chemical activation agent: char ratio of 1:1) for vacuum dried (4 h) impregnation procedure.

for the normal air-dried activated carbons and the vacuum dried activated carbon is shown in Table 5. A significant increase in porosity and decrease in yield is observed for the activated carbon produced via the impregnation–vacuum drying process compared with the activated carbons produced with the impregnation-air drying process. This data, suggests that significant carbonation of KOH occurs during the air drying phase of the impregnation procedure.

3.3. Influence of the activating agent on gaseous evolution

Further investigation of the differences between alkali hydroxides (KOH and NaOH) and alkali carbonates (K_2CO_3 and Na_2CO_3) as activating agents was undertaken. The differences in the gas evolution in relation to time/temperature during the chemical activation process was undertaken in relation to the alkali hydroxides, KOH and NaOH and in relation to the alkali carbonates, K_2CO_3 and Na_2CO_3. The biomass flax pyrolysis chars (1.00 g) were impregnated with 4:1 ratios of KOH and NaOH and dried in a vacuum oven for 4 h to prevent carbonation. Similar procedures were carried out for the two carbonates but the chemical loadings were adjusted to ensure a constant metal:char content when compared to the hydroxide samples (4.92:1 and 5.33:1 for K_2CO_3 and Na_2CO_3 respectively). The impregnated chars were then chemically activated by heating at 5 °C min^{-1} to the activation temperature of 800 °C and held at 800 °C for 2 h. The gas evolution profiles in relation to time/temperature during the chemical activation process are shown in Fig. 5 for the hydroxides (KOH and NaOH) and in Fig. 6 for the carbonates (K_2CO_3 and Na_2CO_3). The total mass of the individual gases released for each activating agent and the untreated char are shown in Table 6.

Table 5
Surface area and porosity characteristics of the alkali chemically activated carbons.

Sample	A_{BET} [m^2/g]	V_{MIC} DR-N_2 [cm^3/g]	V_{MIC} DR-CO_2 [cm^3/g]	V_{MES} [cm^3/g]	Yield [%]
KOH	1051	0.411	0.377	0.122	79
K_2CO_3	1007	0.399	0.357	0.117	76
KOH (vac)	1197	0.460	0.401	0.129	64

The gas evolution profiles clearly show significant differences in the activation process between the hydroxide and carbonate chemical activating agents. The hydrogen peaks for the hydroxide samples occur at much lower temperatures (600 °C for KOH and 625 °C for NaOH) when compared to the carbonate samples (both occurring at an activation temperature of 800 °C). The total gas quantities evolved shown in Table 6 are also far greater. For carbon monoxide, the gas evolution profiles peak at similar activation temperatures for all the samples but the total amounts of gas (Table 6) are considerably reduced for the two hydroxide samples.

In addition, CO production commences at lower temperatures (500 °C) for the carbonate activating agents. The carbon dioxide profiles are again reduced considerably when activating the char with KOH and NaOH. Indeed, the total CO_2 production for these samples is not significantly greater than for the untreated char. For comparison, Yamashita and Ouchi [24] compared the evolution of gases when activating 3,5-dimethylphenol-formaldehyde resin with various alkali metal salts. They reported that evolution of hydrogen was far greater with NaOH and KOH than for the corresponding carbonates.

3.4. Activated carbon porosity in relation to gas evolution

The results have shown that there are significant differences in the quantities of gaseous products released during the activation process

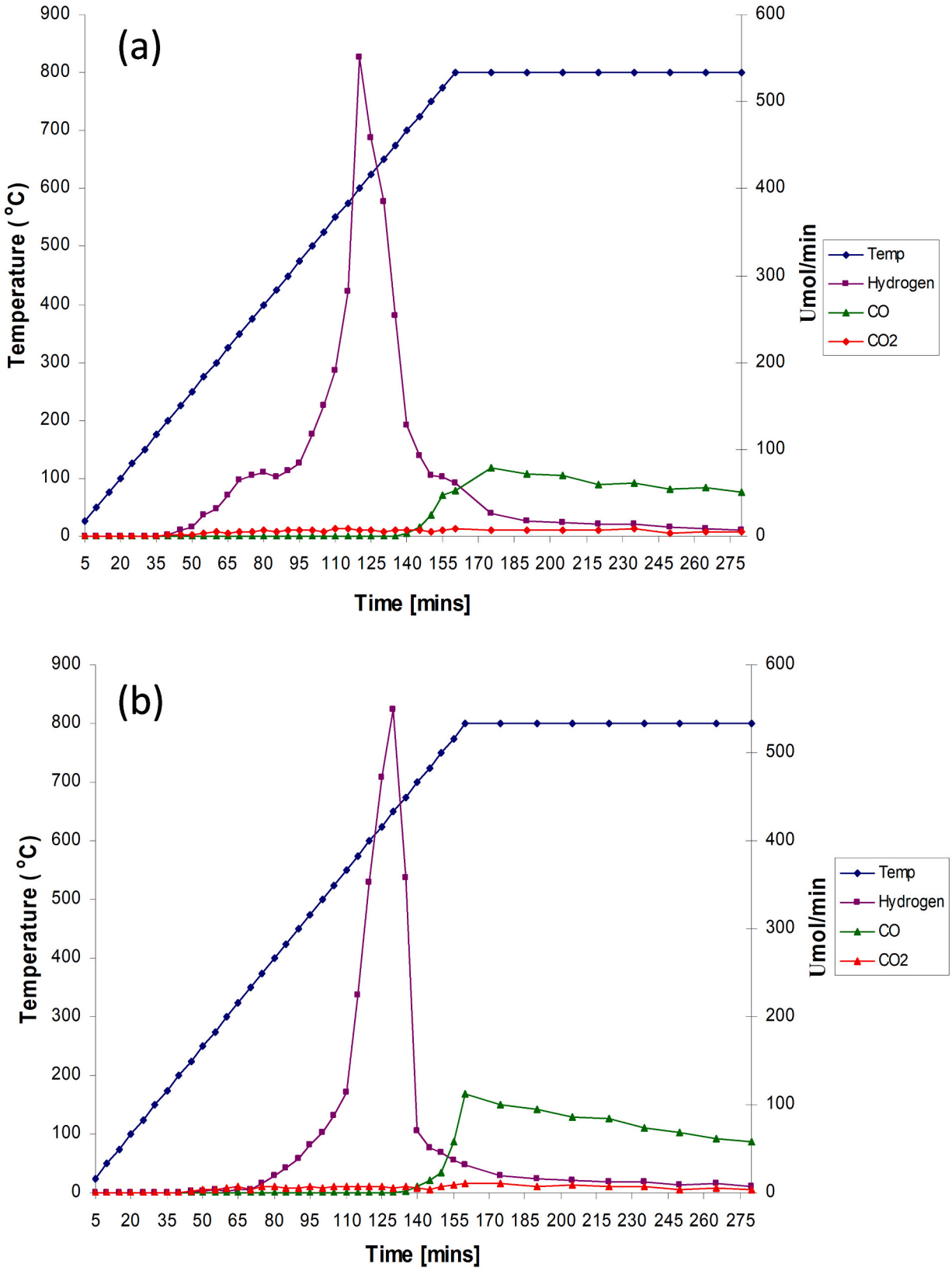

Fig. 5. Product gas evolution in relation to time/temperature for pyrolysis char (produced at pyrolysis temperature 800 °C) for vacuum dried (4 h) impregnation procedure (a) 4:1 ratio for KOH (b) 4:1 ratio for NaOH.

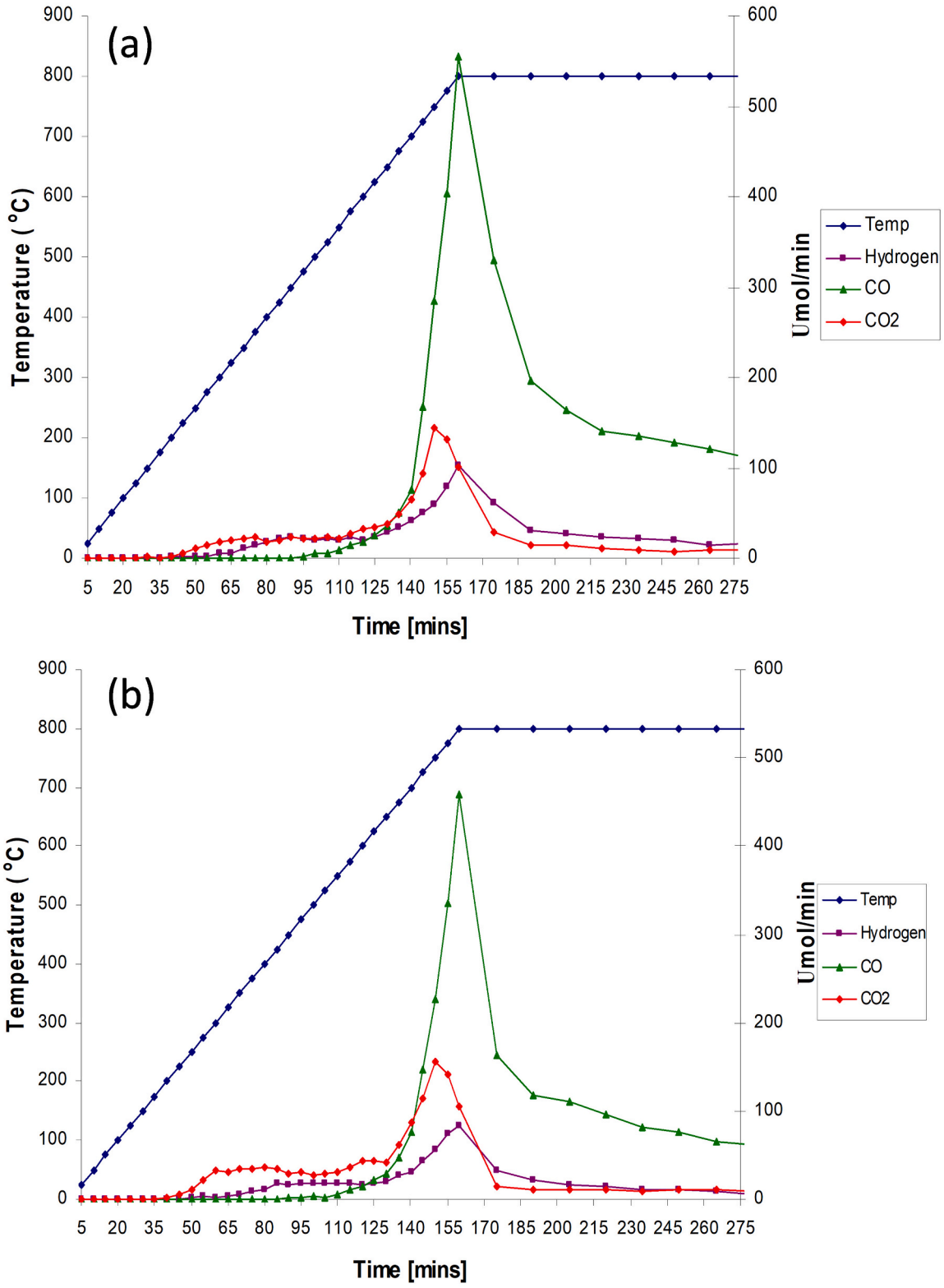

Fig. 6. Product gas evolution in relation to time/temperature for pyrolysis char (produced at pyrolysis temperature 800 °C) for vacuum dried (4 h) impregnation procedure (a) 4.92:1 ratio K_2CO_3 (b) 5.33:1 Na_2CO_3.

with alkali hydroxides compared with the corresponding carbonates, thereby suggesting a difference in the activation mechanism. To further understand the process, the development of the porosity in the product activated carbon was undertaken. The activation process was stopped at various temperatures and the activated carbon at that stage of the activation process was removed from the reactor system and analysed in terms of surface area and porosity. The procedure consisted of: biomass flax pyrolysis char (1.00 g) was impregnated with 4.00 g of KOH and then dried for 4 h in a vacuum oven to prevent the carbonation reaction. The samples were then activated by heating under identical conditions but with the activation stopped at 450, 650 and 800 °C without any hold time, followed by the same post-activation procedure as before. Further

Table 6
Total mass of evolved gases during alkali metal salt chemical activation.

Sample	Quantity released (mg)		
	CO	CO_2	H_2
Untreated	65	52	5
1:1 KOH	473	170	11
1:1(eq^t) K_2CO_3	454	168	11
1:1 KOH**	595	47	15
4:1 KOH**	227	66	38
4:1(eq^t) K_2CO_3	842	303	14
4:1 NaOH**	297	67	30
4:1(eq^t) Na_2CO_3	570	345	9

KOH prepared pyrolysis char samples were heated to the final activation temperature of 800 °C and withdrawn after 1 and 2 h hold time. The porosity of the samples was assessed by adsorption of N_2 at 77 K and CO_2 at 273 K. The determination of the adsorption isotherms would allow accurate assessment of porosity development during the early stages of activation. The yield of activated carbon and of the activating chemical was also assessed. Figs. 7 and 8 show the CO_2 and N_2 adsorption isotherms and corresponding DFT size distribution profiles respectively. Table 7 shows the surface area and porosity data for the prepared carbons.

Fig. 7 shows that up to the activation temperature of 450 °C, the porosity of the activated carbon has only increased slightly in comparison to the flax char. Considerable porosity development is observed between activation temperatures of 450 and 650 °C. Fig. 5(a) showed that in the case of KOH, the gas evolution profiles show that the main evolution of hydrogen gas also occurs between 450 and 650 °C activation temperature. This appears to be a stage of pore creation as the micropore size distribution (CO_2) remains similar to the 450 °C activation temperature carbon sample. However, there is evidence of an increase in the accessibility of the narrow pores to nitrogen (77 K) (Table 7, DR values) possibly via the removal of constrictions at the pore entrances. The characteristics of the activated carbons produced at 650 and 800 °C, show that there is again a considerable increase in porosity although this is less marked than that observed between the activation temperatures of 450 and 650 °C. In addition, pore widening has become a feature of the process. This can be clearly seen in the shape of the CO_2 isotherms and corresponding DFT profiles (Fig. 7(a) and 7(b)). The pore width peak between 3 and 4 Å declines to below the level of the 650 °C activated carbon sample whereas the pore width peak between 5 and 6 Å becomes taller and broader (Fig. 7(b)). During the hold period of the activation process at 800 °C, the micropore distribution becomes more heterogenous and widening of the existing micropores appears to be the dominant process. The pore width peak at 3 to 4 Å (Fig. 7(b)) has disappeared completely for the sample with 2 h hold with a large increase in the contribution from pores above 7 Å pore width. The same trend is shown in the DFT plots for the N_2 adsorbate (Fig. 8(b)). The creation of narrow micropores at low temperatures followed by pore widening at higher temperatures has also been observed by others. For example, Otowa et al. [25] activated coconut shell char at 4:1 ratio KOH and observed a considerable increase in narrow micropores (<10 Å) between activation temperatures of 400 and 600 °C. Further increases in temperature saw a decline in such pores with a considerable increase in larger micropores and mesopores. Ahmadpour and Do [26] and Teng and Hsu [27] studied the activation of bituminous coals with KOH. Both studies reported considerable development of microporosity between 500 and 700 °C. The latter study showed that pore widening became a feature above 600 °C. Evans et al. [28] also noted considerable development of microporosity between 400 and 600 °C when activating a sucrose char (prepared at 675 °C) at KOH loading of 4:1.

The development of the porosity in the activated carbons in relation to activation temperature was also undertaken with K_2CO_3 chemical activation at activation temperatures of 450, 650 and 800 °C. The chemical loading of the char with K_2CO_3 was 4.92:1 to maintain a consistent potassium content compared to the KOH samples. Figs. 9 and 10 show the adsorption isotherms and corresponding DFT plots for the K_2CO_3 activated carbons. Table 7 shows the surface area and porosity data for the prepared carbons using K_2CO_3. The results illustrate clear differences in the porosity development for the K_2CO_3 compared to the KOH activating agents as also suggested by the gas analysis (section 3.1). For KOH, pore formation commences below the activation temperature of 450 °C, corresponding to the production of hydrogen (Fig. 5(a)). For K_2CO_3, the onset of activation occurs at a higher temperature of around 650 °C. This coincides with the main peaks for CO and H_2 evolution, which occur simultaneously (Fig. 5(b). There is some release of CO_2 and H_2 at lower temperatures but this is accompanied by only a slight increase in the porosity of the carbon.

Under the conditions studied here, KOH is a more effective activating agent than K_2CO_3. Porosity development is greater at all stages of the process, both as a function of activation temperature (Table 7) and char burn-off (Fig. 11). Burn-off is here described as the loss of char mass due to the chemical activation process. The widening of the microporosity also becomes significant earlier in the pore development process when activating with K_2CO_3 as reflected by the DR values for the two different adsorbates (Table 7). Hence, for activated carbons with similar micropore volumes, the micropore size distribution will be more heterogenous for K_2CO_3 activated samples than those prepared with KOH. Pore widening coincides with the production of CO for both activating chemicals. With KOH, pore creation seems to be the major process prior to the commencement of CO production and seems to be related to the production of H_2. The main production of CO and H_2 occurs simultaneously for K_2CO_3 and this may explain why pore-widening becomes a feature at an earlier stage in the formation of porosity as pore creation and widening are also taking place simultaneously. Direct comparisons of porosity development in activated carbons produced from KOH and K_2CO_3 have been studied by others. For example, Hayashi et al. [29] prepared chemically activated carbons from lignin at temperatures from 500 to 900 °C. Using KOH, porosity development commenced below 500 °C whereas K_2CO_3 activation required higher temperatures. In contrast to the current work, higher pore volumes were observed for K_2CO_3 at temperatures of 700 °C and above. Okada et al. [30] activated waste newspaper between 700 and 900 °C. Higher surface areas and total pore volumes were observed for KOH up to 850 °C, with K_2CO_3 more effective at higher temperatures.

3.5. Development of porosity during alkali metal salt activation

Comparison was made of the actual pore development observed for the KOH and K_2CO_3 carbons with the theoretical pore development based on the burn-off of the samples during activation. The theoretical porosity was calculated according to Eq. (3). For the purpose of the calculation, it was assumed that burn-off resulted only in pore creation and potential surface erosion effects were neglected. The true solid density of the char was taken to be 2.20 g cm^{-3}, based on the solid density of graphite. This was considered preferable to the use of the char helium density (1.86 g cm^{-3}), as the low measured value suggested the possible presence of closed porosity.

$$V_{TP} = (V_C + (1/\rho_C \times Q/100)) \times 100/(100 - Q) \quad (3)$$

where: V_{TP} = Theoretical pore volume of activated carbon (cm^3/g).

V_C = Total pore volume of un-activated char by N_2 adsorption (cm^3/g).

ρ_C = true density of un-activated char (2.20 g/cm^3).

Q = Burn-off during activation (%).

Fig. 12 compares the theoretical pore development (Eq. 3) with the actual development of porosity as determined by adsorption of nitrogen at 77 K. Fig. 12 shows the data for the chemically activated carbons and also for comparison the physically activated carbons produced by activation with CO_2. In the early stages of burn-off, the experimental data

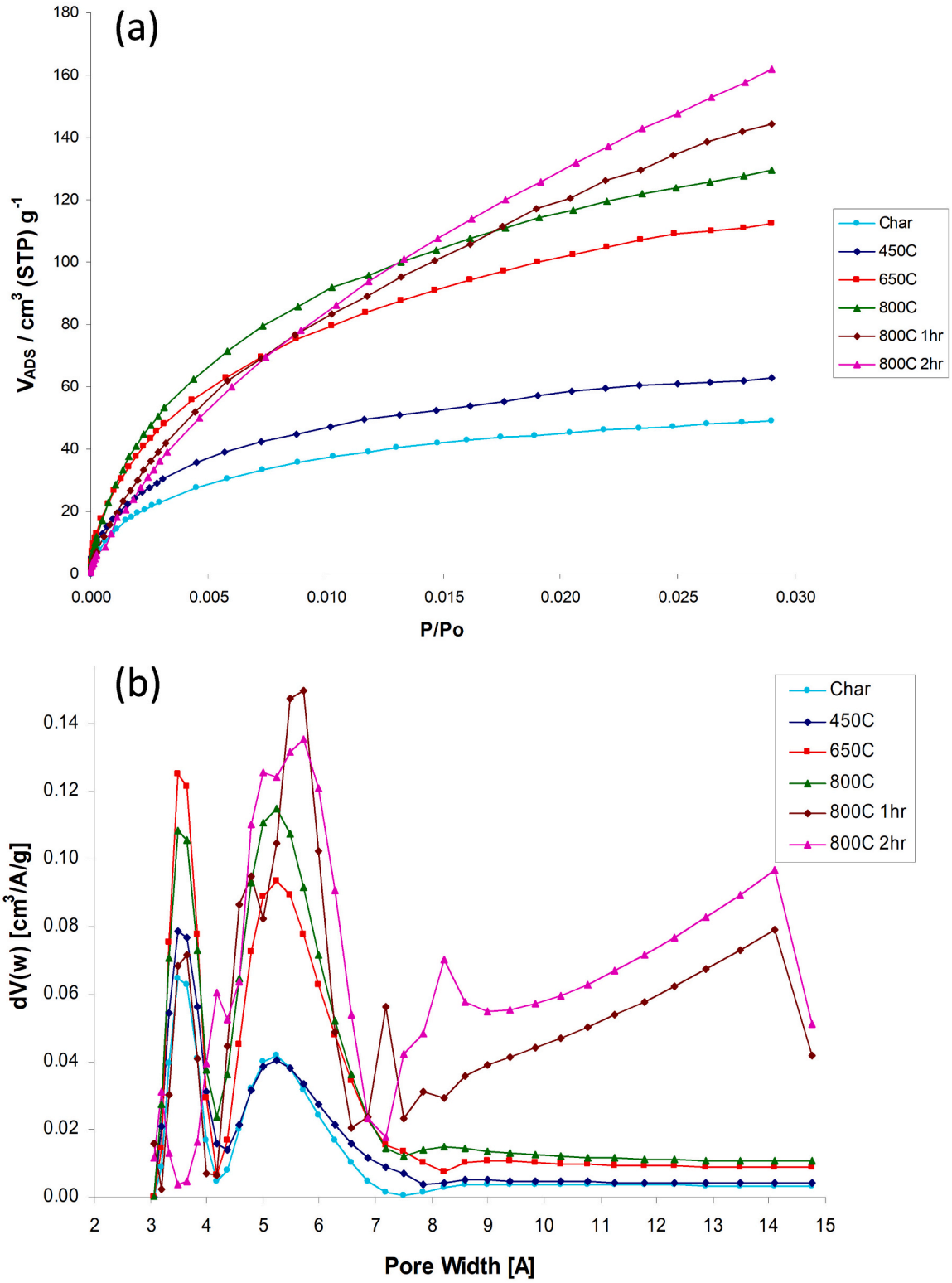

Fig. 7. (a) CO_2 isotherms at 273 K; porosity development in relation to activation temperature for activated carbons (KOH 4:1) (b) CO_2 DFT micropore size distribution development in relation to activation temperature for activated carbons (KOH 4:1).

shows porosity development exceeding the theoretical predictions for all methods of activation. This is especially marked for the KOH and K_2CO_3 processes and provides a strong indication that the creation of pores is not solely reliant on the consumption of material from the char. In the latter stages of the activation process, the development of pores per unit burn-off is lower and the difference between the measured and theoretical values is considerably reduced. This suggests that surface erosion of the chars becomes more significant at high burn-off and creation of new pores is significantly reduced.

Fig. 13 shows the helium density of the KOH and K_2CO_3 activated carbons as a function of char burn-off. Data for the physically activated (CO_2 activating agent) samples are also shown for comparative

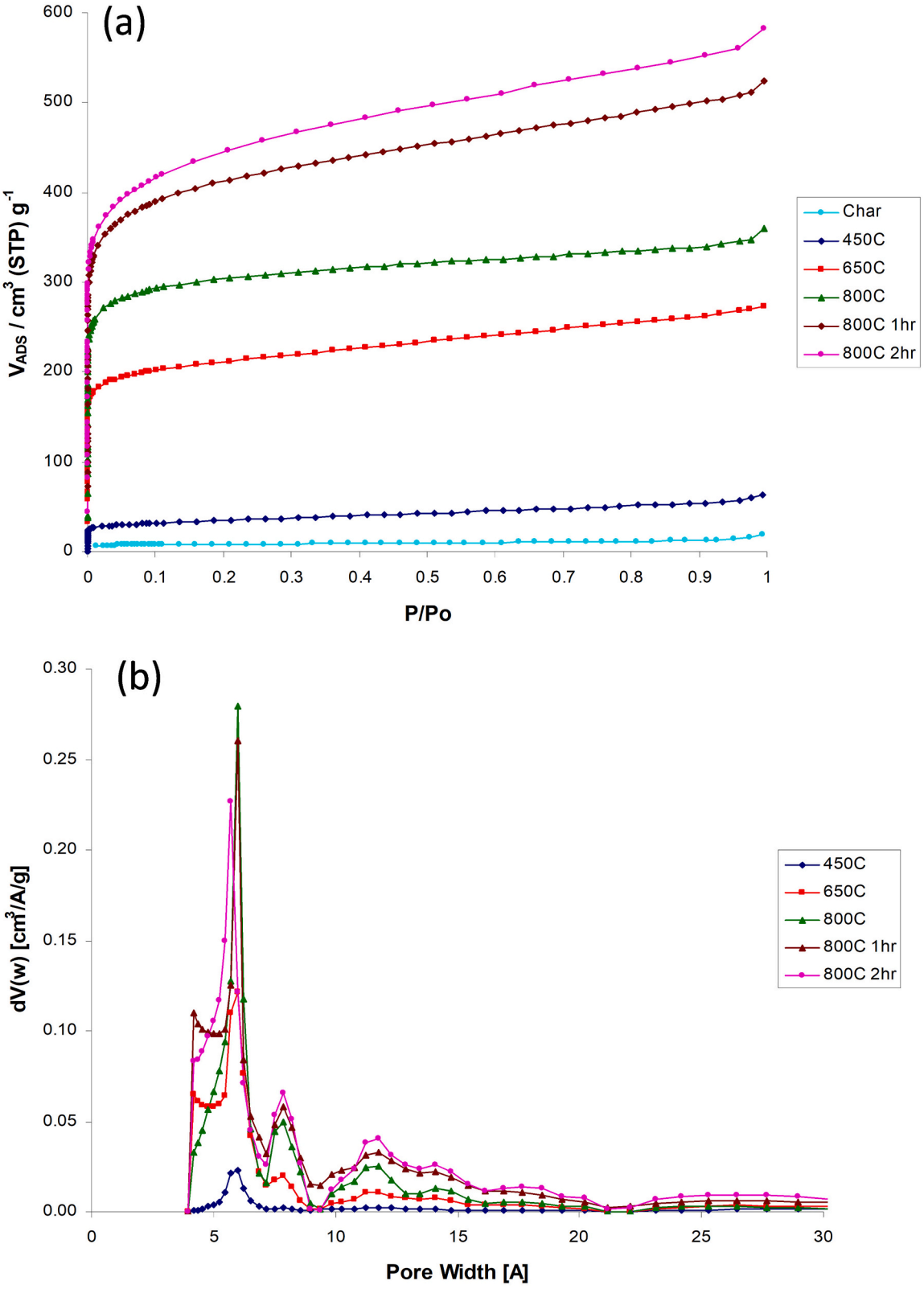

Fig. 8. (a) N_2 isotherms at 77 K; porosity development in relation to activation temperature for activated carbons (KOH 4:1) (b) N_2 DFT micropore size distribution development in relation to activation temperature for activated carbons (KOH 4:1).

purposes. The KOH and K_2CO_3 samples show similar trends with an initial sharp increase in helium density at low burn-off (up to around 20%) followed by a more gradual increase at higher burn-off values. The physically activated samples show a more or less linear increase in density over the whole range of burn-off. Such increases in density may be explained by the opening of closed porosity present in the char precursor (ie. where previously inaccessible pores are made available to the helium) or by accumulation of inorganic impurities (ash) in the carbon

Table 7
Porous texture data for KOH and K_2CO_3 activation (4:1 ratio eq[t]).

Chemical agent	Temp [°C]	V_{MIC} DR-N_2 [cm^3/g]	V_{MIC} DR-CO_2 [cm^3/g]	A_{BET} [m^2/g]	Yield [%]
Untreated	n/a	0.012	0.151	30	n/a
KOH	450	0.050	0.170	126	98
K_2CO_3	450	0.011	0.153	31	100
KOH	650	0.309	0.332	807	94
K_2CO_3	650	0.026	0.165	45	99
KOH	800	0.451	0.422	1177	83
K_2CO_3	800	0.232	0.273	607	90
KOH	800 1 h	0.604	0.458	1564	67
K_2CO_3	800 1 h	0.377	0.346	985	78
KOH	800 2 h	0.639	0.464	1656	57
K_2CO_3	800 2 h	0.424	0.347	1105	55

structure during activation.

Fig. 14 shows the ash content of the activated carbons as a function of burn-off. The theoretical ash content, based on the assumption that no mineral matter is lost from the char during activation, was calculated according to Eq. (4).

$$X_{ACT} = (100/(100 - Q)) \times X_C \quad (4)$$

Where; X_{ACT} = ash content of activated carbon (%).
X_C = ash content of un-activated char (%).
Q = burn-off during activation (%).

For both the KOH and K_2CO_3 activated samples, the ash content remains fairly stable over the range of burn-off. This suggests that inorganic material is removed, either during the activation or the ensuing washing procedure, and that the observed increase in helium density is unlikely to be a result of the accumulation of inorganic impurities. Therefore, it may be suggested that the opening of closed pores is responsible for the increase in density. In contrast, the physically activated samples show an increase in ash content that closely follows the theoretical prediction, thus showing that mineral matter is retained in the carbon matrix during physical activation, as also shown in our previous work [19].

Fig. 15 shows the fixed-carbon content of the KOH and K_2CO_3 activated flax carbons as a function of burn-off. The chemically activated samples show a dramatic increase in fixed-carbon content at low burn-off, thus corresponding with the main changes in porosity and helium density. A decline in the volatile matter content was also observed. This indicates that the activating agent is reacting preferentially with disorganised/volatile material during the early stages of the activation, where the creation of pores is the predominant process. During the latter stages of the activation at high burn-off, the fixed-carbon content begins to decline, probably as a result of burn-off of the fixed-carbon matrix and an increase in the ash content. This period was characterised by a widening of the existing porosity (section 3.4). Similar trends for fixed carbon and helium density were observed by Yang and Lua [31] during activation of pistachio-nutshell chars with KOH. As the activation temperature was increased from 500 to 700 °C, the fixed carbon content increased considerably from 79.1 to 87.7% with a less marked increase to 88.1% as the temperature was increased further up to 900 °C. This was accompanied by a significant increase in the helium density. As in the current work, the bulk of the micropore development corresponded to the sharp rise in fixed carbon content and helium density observed in the early stages of activation, with pore widening becoming the major process above 700 °C. Yang and Lua [31] also reported only slight reductions in yield (21.2 wt% to 19.6 wt%, expressed as wt% of the original nutshell) were observed between 500 and 700 °C, whereas a large decrease (19.6 to 12.4%) was observed between 700 and 900 °C. Again, this is in agreement with the current work (Fig. 12) where the bulk of the porosity is created at low burn-off. As noted in section 3.4, the creation of porosity in the chemically activated chars appears to be related to the release of hydrogen gas whereas the release of carbon monoxide coincides with the widening of pores. The data here suggests the removal of volatile and disorganised material is taking place simultaneous with the hydrogen evolution and also pore creation. This suggests that the hydrogen is produced as a product of the reaction between disorganised material in the flax char and the chemical activating agent.

3.6. Mechanism of KOH and K_2CO chemical activation

The mechanism for the chemical activation of biomass by impregnation of the raw biomass material with activating chemicals is typically described as: (i) impregnation produces degradation of the cellulosic material in the precursor or (ii) the chemical agent acts as a dehydrating agent during the heat treatment, producing charring and aromatisation of the carbon skeleton and inhibiting the formation of tars [26,32,33]. However, such mechanisms would not be applicable to a two-step process involving chemical activation of pyrolysis char where major structural changes do not occur during activation and the pore development is inherently related to the structure of the un-activated char. Therefore, an alternate mechanism is suggested here for the chemical activation of biomass pyrolysis char, described in relation to the increase in the temperature of activation.

3.6.1. KOH activation mechanism

The impregnation stage of the activation is often ignored but it is likely that some interaction will occur between the KOH and the char during the mixing and drying stage of the wet impregnation procedure. The presence of functional groups on the surface of the biomass flax pyrolysis chars, particularly acidic oxygen containing groups such as phenol, lactone, carboxylic acid and carboxylic anhydrides will react with the strong alkali solution during the impregnation stage. Reactions 2 and 3 show possible reactions of KOH with carboxylic acid and phenol functionalities:

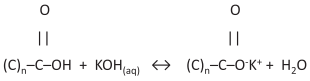

(Reaction 2)

$$(C)_n\text{–}OH + KOH_{(aq)} \leftrightarrow (C)_n\text{–}O^-K^+ + H_2O \quad \text{(Reaction 3)}$$

Such reactions are likely to facilitate an intimate contact between the char and the activating agent. However, they do not appear to influence the porous structure of the carbon and may well be reversible if subjected to the washing procedure. The carbonation of KOH to K_2CO_3 during the drying stage has been shown to be an important factor during extended drying times in air and should be avoided to ensure maximum porosity development during activation. At low KOH ratios, the carbonation may be so extensive that the activation effectively proceeds as a carbonate system.

During the activation process, at activation temperatures of up to 450 °C, significant weight loss (~12 wt%) occurred from the activating chemical. This has been attributed to loss of moisture from dehydration of KOH to K_2O, hygroscopic absorption of moisture by KOH followed by subsequent dehydration during activation, or perhaps loss of some KOH from the sample upon melting (ca 360 °C).

At activation temperatures between 450 and 650 °C, significant changes occurred in the porosity of the char precursor (Table 7). The creation of pores was accompanied by a significant increase in the helium density (Fig. 13), an increase in fixed carbon (Fig. 15) and a decline in volatile matter content of the char. During this period, the development of porosity per unit burn-off far exceeded the theoretical predictions (Fig. 12). Data discussed in Section 3.5 suggested that the bulk of the porosity was created via removal of volatile/disorganised material, thus developing the existing rudimentary pore structure of the char precursor. The gaseous evolution profiles (Fig. 5) demonstrated significant evolution of hydrogen gas between activation temperatures of 450

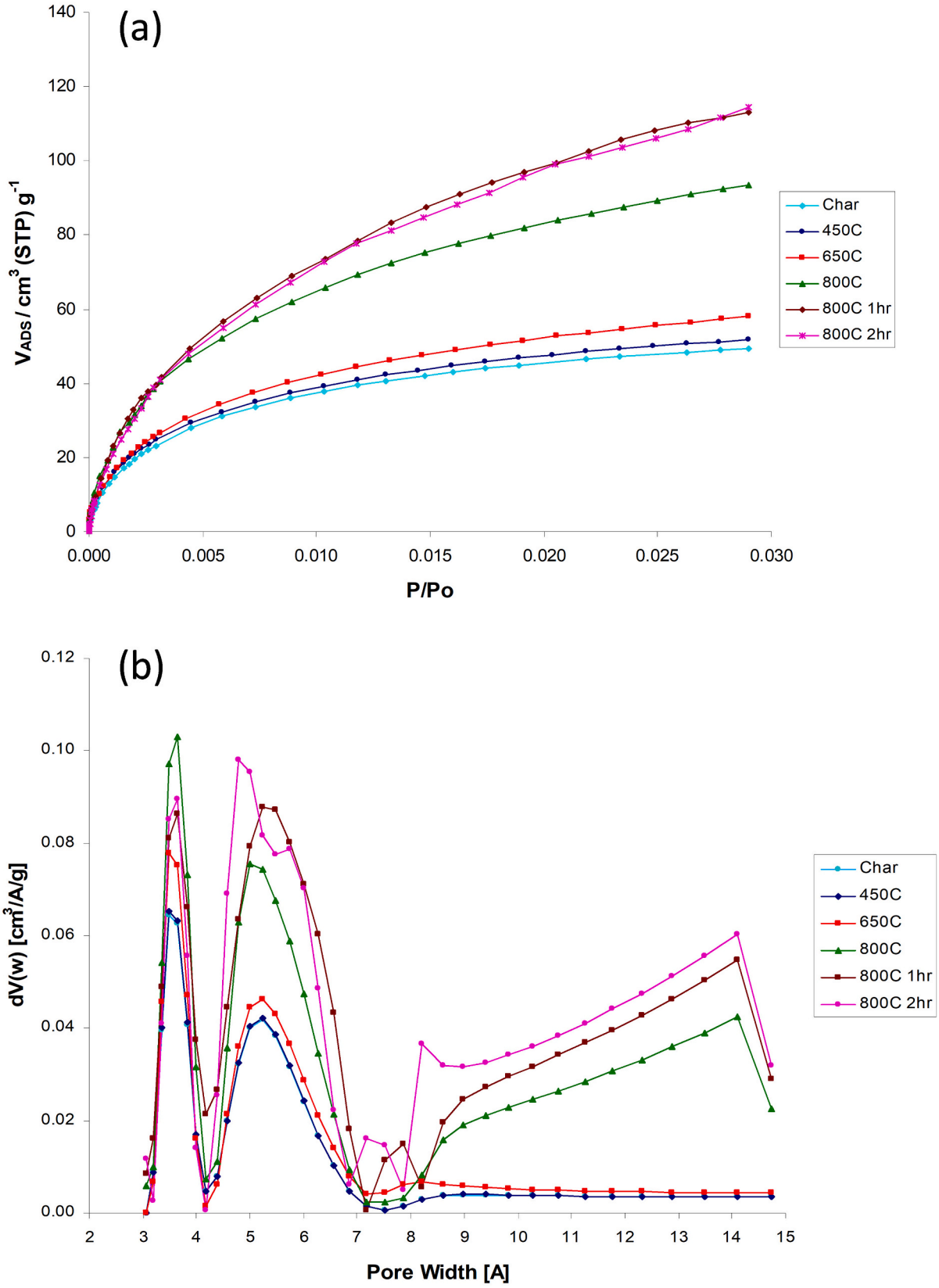

Fig. 9. (a) CO_2 isotherms at 273 K; porosity development in relation to activation temperature for activated carbons (K_2CO_3 4:1) (b) CO_2 DFT micropore size distribution development in relation to activation temperature for activated carbons (K_2CO_3 4:1).

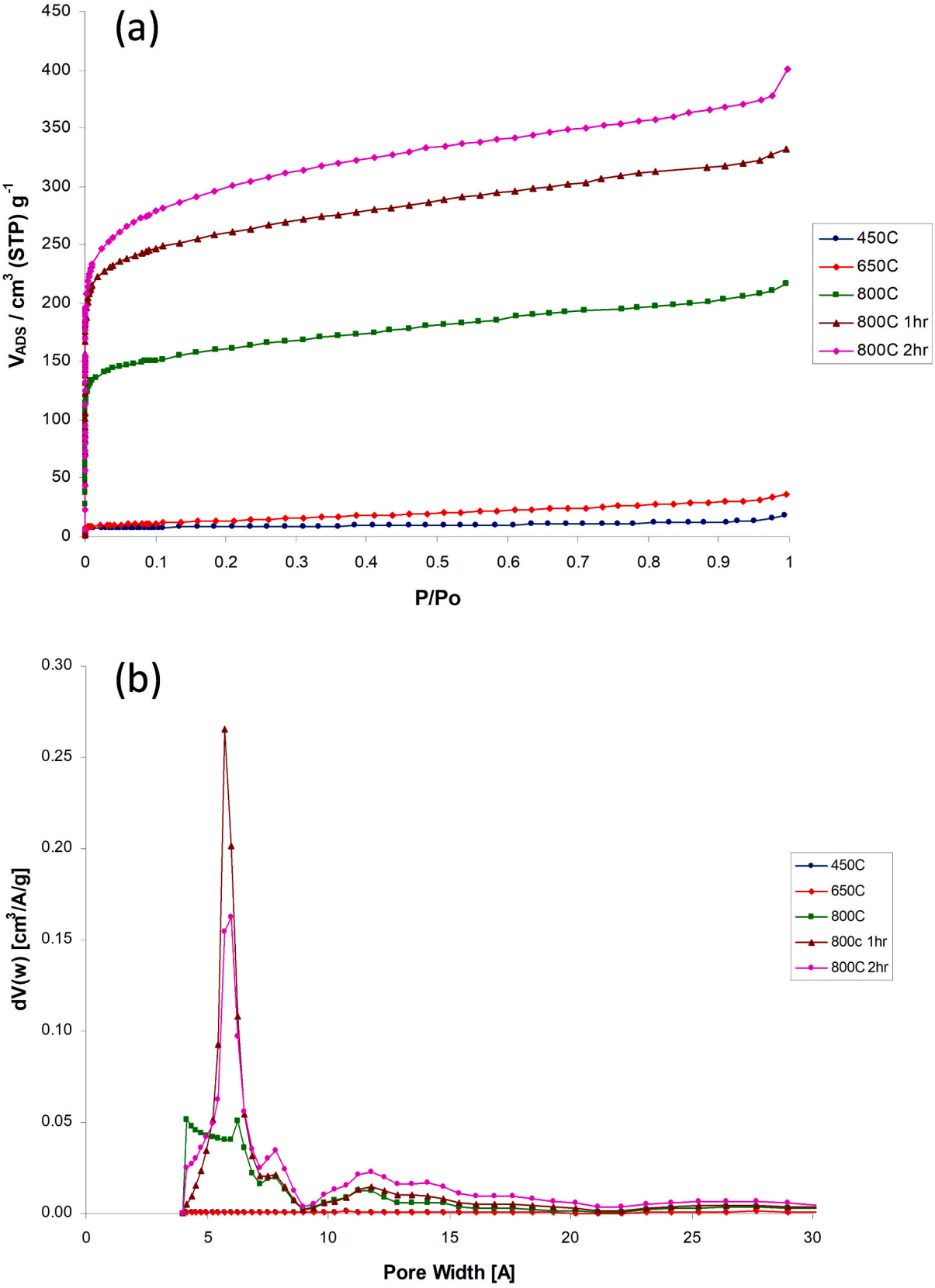

Fig. 10. (a) N_2 isotherms at 77 K; porosity development in relation to activation temperature for activated carbons (K_2CO_3 4:1) (b) N_2 DFT micropore size distribution development in relation to activation temperature for activated carbons (K_2CO_3 4:1).

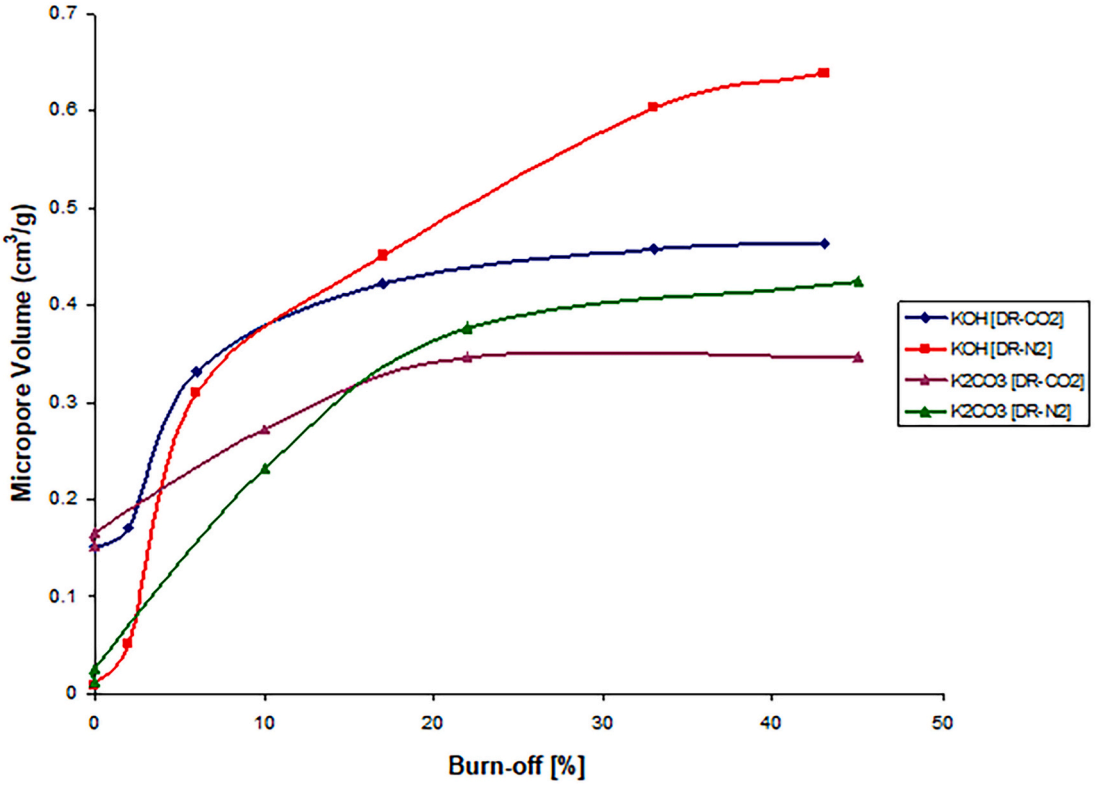

Fig. 11. Development of microporosity as a function of burn-off.

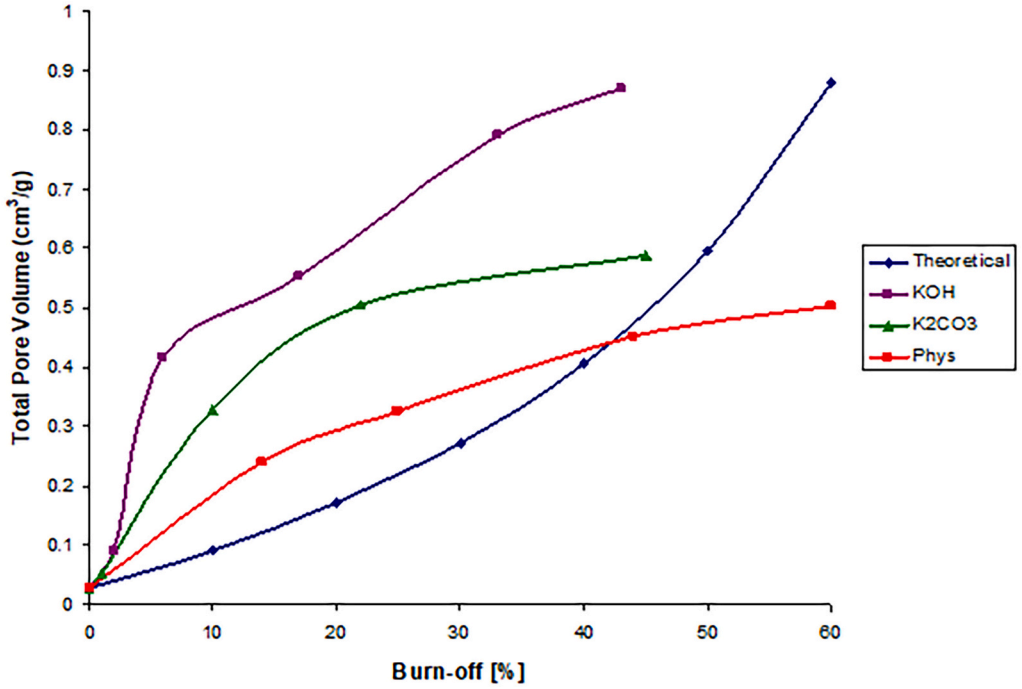

Fig. 12. Development of porosity; Experimental versus theoretical.

and 650 °C corresponding to reactions involved in the development of micropores through direct reaction between the KOH and the pyrolysis char. The melting points of KOH and K_2O are 360 and 350 °C respectively with K_2O decomposing to give metallic potassium and potassium peroxide (Reaction 4). Metallic potassium is in the liquid phase above 63 °C and the peroxide melts without decomposition at 490 °C [34].

$$4\,K_2O_{(l)} \rightarrow 4\,K_{(l)} + 2K_2O_{2(l)} \qquad \text{(Reaction 4)}$$

At activation temperatures in excess of 360 °C, the presence of an alkali liquid consisting predominantly of KOH would be expected. This is likely to exist in the form of an ionic melt, and may also contain metallic potassium and potassium oxides [35], The creation of

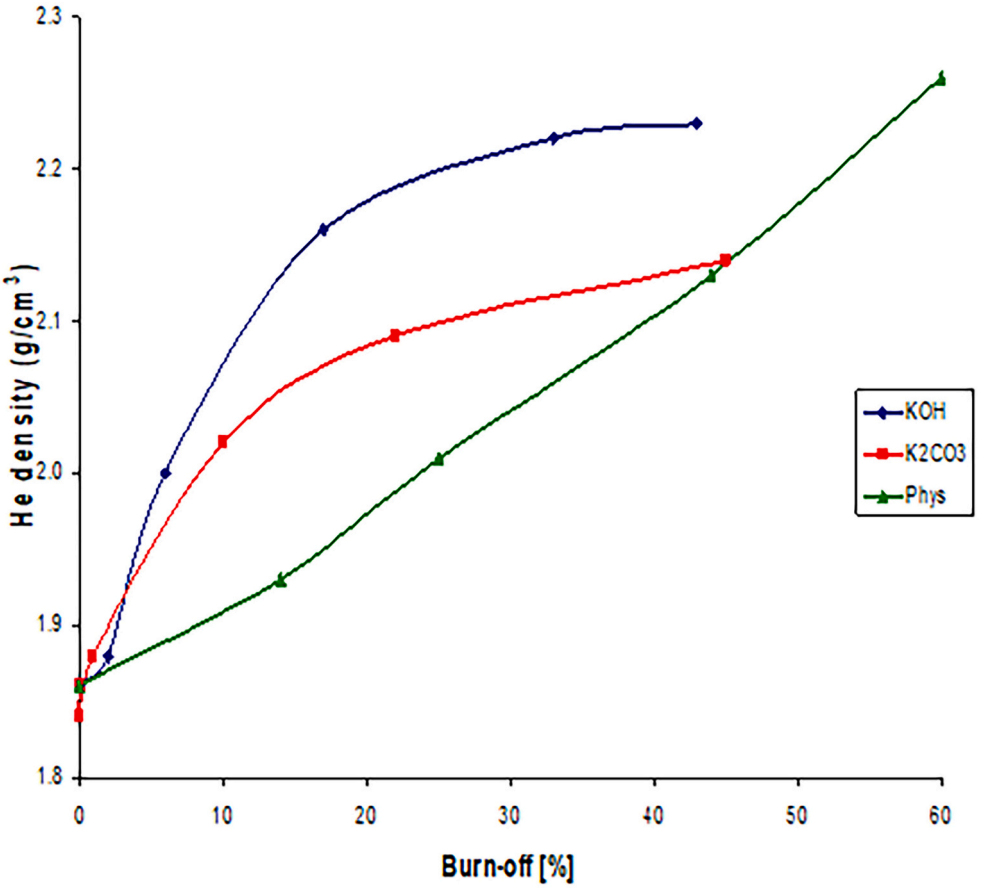

Fig. 13. Helium density of activated carbons as a function of burn-off.

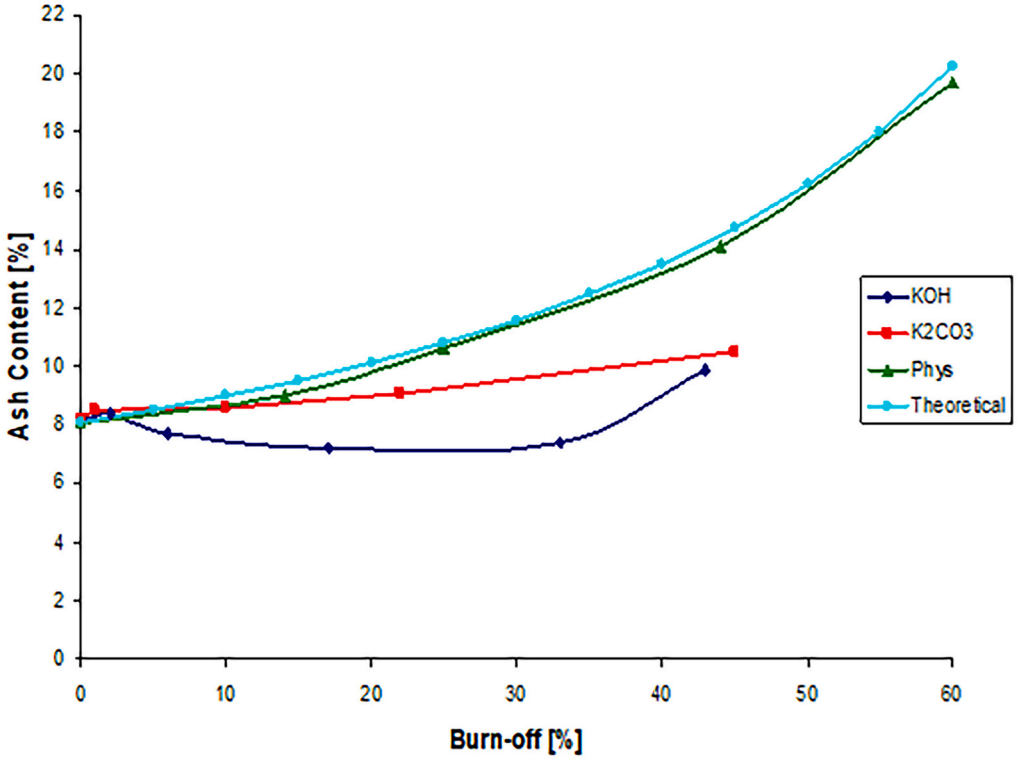

Fig. 14. Ash content of activated carbons as a function of burn-off.

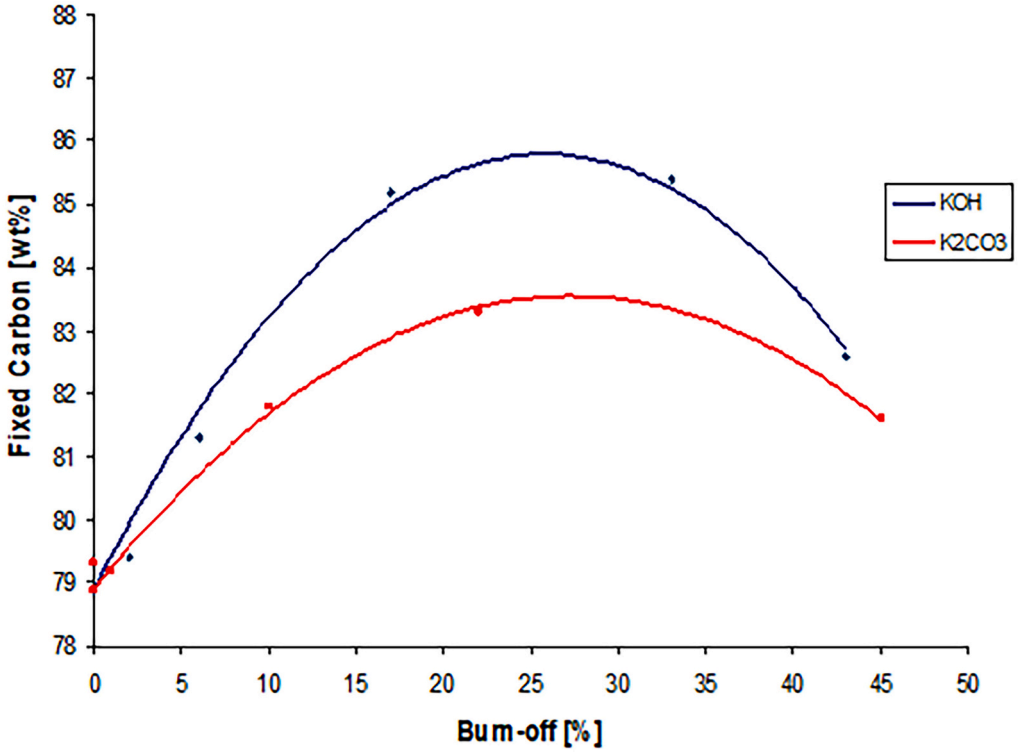

Fig. 15. Fixed-carbon content of chemically activated carbons as a function of burn-off.

micropores and evolution of hydrogen commenced at a temperature around the melting point of the KOH, probably as a result of the reaction between the alkali melt and disorganised/volatile material in the precursor. The gaseous evolution profiles (Fig. 5) showed little release of gaseous carbon (as CO and CO_2) below 700 °C despite significant losses of carbon from the char over the same activation temperature range, indicating the formation of a carbon containing potassium compound, presumably K_2CO_3. Lillo-Rodenas et al. [36] proposed a global reaction for KOH/NaOH activation based on the activation of anthracite (Reaction 5).

$$6\,K/NaOH + C \leftrightarrow 2\,K/Na + 3H_2 + 2Na_2/K_2CO_3 \quad \text{(Reaction 5)}$$

The reaction was proposed to commence at around 560 °C for NaOH and 400 °C for KOH, in accordance with the release of hydrogen. As in the current work, carbon was not released in the gaseous phase below 700 °C suggesting formation of carbonate was occurring simultaneously to the production of hydrogen. Yamashita and Ouchi [37] suggested the evolved hydrogen to be a product of the reaction between the alkali metal compounds and hydrogen containing groups (eg methylene groups) and/or aromatic hydrogen on the carbon surface (Reactions 6 and 7).

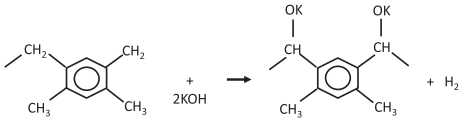

(Reaction 6)

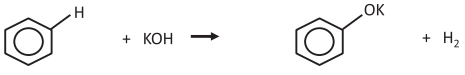

(Reaction 7)

Reactions 6 and 7 suggest that at least 50% of evolved hydrogen originates from the char. However, the data from Section 3.4 suggests that this is not the case, with over 90% originating from the KOH at 650 °C. This phenomenon may be explained by the formation of oxygen and hydrogen containing complexes at certain sites on the char surface by transfer of atoms from the molten metal/metal oxide phase. This is likely to occur in positions where carbon atoms possess unpaired electrons or residual valency's, such as the edges of the twisted aromatic sheets and at sites where dislocations and defects exist [32]. Reaction 8 shows a possible reaction.

$$\equiv C_X + K^+OH^-_{(l)} \rightarrow \equiv COH + K^+_{(l)} \quad \text{(Reaction 8)}$$

where C_X = carbon site with a free sp^2 electron.

The COH functionalities formed can then react according to Reactions 9 and 10, thus generating hydrogen solely from the activating agent.

$$2(\equiv COH) + 2\,K^+_{(l)} \rightarrow 2(\equiv CO^-K^+) + H_{2(g)} \quad \text{(Reaction 9)}$$

$$\equiv COH + KOH_{(l)} \rightarrow \equiv CO^-K^+ + H_2O_{(g)} \quad \text{(Reaction 10)}$$

The recycling and interchanging of the potassium compounds with product gases in the reactor according to Reactions 11 and 12 is also likely.

$$K_2O + H_2 \leftrightarrow 2\,K + H_2O \quad \text{(Reaction 11)}$$

$$2\,K + 2H_2O \leftrightarrow 2KOH + H_2 \quad \text{(Reaction 12)}$$

The burn-off of carbon material from the char can be presumed to be related to the decomposition of the potassium groups with the release of carbon monoxide (Reaction 13) and potassium metal, which may develop further porosity via intercalation. Alternatively, it may continue to react as in Reactions 9 and 12, inferring a cyclic process.

$$2(\equiv COK) \rightarrow 2CO + 2\,K \quad \text{(Reaction 13)}$$

The majority of the carbon consumed from the precursor is not released in the gaseous phase. Therefore, as the potassium functionalities decompose, much of the carbon released must be incorporated in the molten metal/metal oxide phase. It is known that alkali peroxides can react with CO according to Reaction 14. Under standard conditions CO behaves as a neutral oxide, but at high temperatures can take on the characteristics of an acidic oxide and react with alkalis [38]. The capability of CO to reduce metal oxides at elevated temperatures is also

reported [39,40]. Potential reactions of CO with the molten alkali phase are shown in Reactions 14 to 18, resulting in the formation of K_2CO_3 as the main reaction product. Under certain conditions, the carbonate may then decompose according to Reaction 19, releasing CO_2 and recycling the oxide to the molten phase. It should also be noted that hydrogen may be generated independently of the precursor as a result of these reactions.

$$K_2O_2 + CO \rightarrow K_2CO_3 \quad \text{(Reaction 14)}$$

$$2KOH + CO \rightarrow K_2CO_3 + H_2 \quad \text{(Reaction 15)}$$

$$CO + K_2O \rightarrow CO_2 + 2\,K \quad \text{(Reaction 16)}$$

$$2KOH + CO_2 \rightarrow K_2CO_3 + H_2O \quad \text{(Reaction 17)}$$

$$H_2O + 2\,K \rightarrow H_2 + K_2O \quad \text{(Reaction 18)}$$

$$K_2CO_3 \rightarrow K_2O + CO_2 \quad \text{(Reaction 19)}$$

The absorption of CO by the bulk molten phase may explain the later release of CO when compared to the carbonate activation. As the quantity of K_2CO_3 in the system increases and the rate of CO release from the char begins to rise, the capacity of the molten phase to incorporate evolved CO would reduce. As a result, the presence of CO in the product gases becomes significant. This corresponds with the end of the main period of hydrogen production where, according to Reactions 14 to 18, significant amounts of K_2CO_3 have been formed in the reactor. Yamashita and Ouchi [41] monitored the gaseous evolution when heating a variety of different coals with NaOH, they also showed that the main temperature of the H_2 production varied with the type of coal and the production of CO always commenced as the H_2 declined.

At higher activation temperatures above 700 °C significant pore widening is observed (Fig. 7) during KOH activation and is likely to result from a combination of different factors. The gasification reactions of carbon with steam and/or carbon dioxide become increasingly favoured thermodynamically at higher temperatures and, considering the porosity already created at lower temperatures, would be expected to widen the existing pore structure. Reactions capable of generating these gasification agents are shown in Reactions 10, 11, 16, 17 and 19. The presence of metallic potassium was proposed at temperatures above 360 °C and the development of pores via formation of intercalation compounds may also occur. Hence, the evaporation of potassium from within the char could lead to structural expansion and a widening of existing porosity.

3.6.2. K_2CO_3 reaction mechanism

For chemical activation of the biomass pyrolysis char with K_2CO_3, the reactions occurring during the wet impregnation stage are likely to proceed in a similar manner to those described for KOH, thus facilitating a good contact between the activating agent and the biomass flax pyrolysis char. No significant development of porosity is observed at this stage. At activation temperatures below 650 °C the K_2CO_3 impregnated chars would be expected to show little change in porosity or carbon yield (Table 7). Small amounts of carbon dioxide and hydrogen are evolved during this period, with the CO_2 originating from the carbonate (e.g. Fig. 6), due to the thermal decomposition of the carbonate in the presence of carbon (Reaction 19). This reaction occurs where intimate contact has been established between the char and the carbonate and may be related to the formation of functional groups during the wet impregnation process. Pure K_2CO_3 melts with decomposition at 896 °C [34], well above the temperatures at which significant CO_2 is observed. The role of K_2CO_3 decomposition (Reaction 19) in chemical activation has also been reported by Mimms and Pabst [42] who showed that K_2CO_3 reacts with coal or char at around activation temperatures of 475 °C with liberation of CO_2 from carbonate and with the formation of surface salt complexes. These complexes, for example, phenoxide groups (C-O-K), may be considered as highly dispersed K^+ species which form at the active sites in the char structure similar to those formed during activation with KOH.

When the temperature exceeds 350 °C (ie. the melting point of K_2O) the reaction between the liquid oxides and the char may commence via the formation of the potassium complexes within the carbon structure and is accompanied by the generation of hydrogen gas. The evolution of CO_2 commences before that of H_2, at temperatures below 300 °C, due to the stability of K_2O at these temperatures, with hydrogen production initiated by the melting and decomposition of the oxide at temperatures around 350 °C. The data described in Section 3.4. suggested that the majority of the hydrogen produced originates from the char, since the K_2CO_3 is not a potential source of hydrogen. The dispersed potassium species may then form according to Reactions 20–23 due to the decomposition of K_2O. In conjunction with the decomposition of K_2CO_3 (Reaction 19) these reactions can release an equimolar mixture of CO_2 and H_2, as observed between 400 and 650 °C (Fig. 6(a)).

$$2K_2O + 2(\equiv CH) \rightarrow 2(\equiv COK) + 2\,K + H_2 \quad \text{(Reaction 20)}$$

$$2\,K + 2(\equiv COH) \rightarrow 2(\equiv COK) + H_2 \quad \text{(Reaction 21)}$$

$$2K_2O \rightarrow 2\,K + K_2O_2 \quad \text{(Reaction 22)}$$

$$K_2O_2 + 2(\equiv CH) \rightarrow 2(\equiv COK) + H_2 \quad \text{(Reaction 23)}$$

The pore development at activation temperatures below 650 °C is restricted by the inactivity of the majority of the potassium carbonate (Table 7). Only small amounts of K_2O have been formed and, as a consequence, only small quantities of dispersed potassium groups can be incorporated within the precursor. The formation of K_2O via decomposition of K_2CO_3 (Reaction 19) can therefore be considered the rate determining step of the activation process.

At activation temperatures above 650 °C, the rate of CO_2 production (and hence carbonate decomposition) increases significantly together with the evolution of hydrogen and carbon monoxide. This coincides with the main period of pore development within the carbon, mainly as a result of the removal of volatile and disorganised material from the char structure. This could occur as a result of the decomposition of the potassium entities (Reaction 24) formed earlier (Reactions 20, 21 and 23). The metallic potassium formed may then react again (Reaction 21), thus resulting in a cyclic process consuming disorganised material in the char. The presence of metallic potassium may also facilitate pore formation via intercalation.

$$2(\equiv COK) \rightarrow 2CO + 2\,K \quad \text{(Reaction 24)}$$

Carbon monoxide may also be produced at higher temperatures by the reaction of carbon dioxide with the char (25).

$$CO_2 + C \rightarrow 2CO \quad \text{(Reaction 25)}$$

Overall, K_2CO_3 activation produces carbons with a lower micropore volume and a wider micropore size distribution for a given degree of burn-off when compared to KOH activation. This is likely to result from a combination of factors. As described above, considerable quantities of CO_2 are present in the system and physical activation of the char (Reaction 25) will take place. For a given degree of burn-off, the physical gasification reaction is less effective in creating micropores than the alkali metal salt activation and will therefore reduce the effectiveness of the process by facilitating pore widening and/or surface erosion of the char. The formation of some CO_2 during KOH activation is also likely but the presence of excess KOH acts as a sink for CO_2, thus reducing the influence of the physical activation reaction. In addition, the bulk of the micropore formation with KOH occurs at lower temperatures (below 700 °C) where the rate of the physical activation reactions is likely to be very slow and hence the two processes are not directly competing. This is facilitated by the low melting point of KOH which allows reaction with the pyrolysis char at lower temperatures than can occur with K_2CO_3, as

decomposition to the oxide (Reaction 19) takes place very slowly at activation temperatures below 650 °C. It may also be suggested that the reaction of volatile/disorganised (and hence more reactive) material will occur preferentially at lower temperatures, as also suggested by the earlier release of hydrogen during activation of more reactive precursors. As the activation temperature is increased the more organised carbon from the main skeleton may also be consumed. The main period of pore creation during carbonate activation takes place at higher temperatures and therefore the alkali/carbon reactions are less selective than for the corresponding KOH system.

4. Conclusions

This work has attempted to understand the mechanism of the chemical activation of biomass flax fibre matting pyrolysis chars with alkali hydroxides and carbonates (KOH and K_2CO_3) for the production of activated carbon fibrous matting. The gaseous products of the different activation systems were quantified as a function of temperature linked to the development of porosity of the activated carbons. Initial experiments highlighted the importance of the impregnation procedure upon the activation process.

For KOH, the activation commenced at activation temperatures of around 350–400 °C with the melting of KOH and the formation of a molten hydroxide/oxide phase. The early stages of the activation involved the selective reaction of disorganised/volatile material from the char with the molten phase, thus developing the existing rudimentary pore structure of the precursor. This process was accompanied by evolution of large quantities of hydrogen gas. During these initial stages, the carbon consumed from the char was not released in the gaseous phase and was incorporated in the molten phase with the formation of K_2CO_3. Mechanisms were proposed for the formation of metallic potassium although the role of intercalation in the creation of pores may be possible. At higher temperatures (>700 °C), pore widening became a significant feature of the process. In addition, the development of porosity per unit carbon burn-off began to decline. This occurred as a result of the consumption of 'fixed' carbon from the aromatic ring structure by physical gasification and/or less discriminate reaction of the alkali molten phase with the char at higher temperatures. It is possible that the boiling of metallic or other potassium species from the char structure may also contribute to the pore widening process.

Activation with K_2CO_3 commenced at higher temperatures (>600 °C) compared to KOH activation and was controlled by the decomposition of the carbonate to K_2O and CO_2. This reaction was facilitated by intimate contact between the char and the activating chemical. Such contact was facilitated by the wet impregnation procedure and may be related to the formation of potassium functionalities. The creation of pores occurred via reaction of the char with the decomposition products of K_2CO_3. The decomposition occurred only slowly below an activation temperature of 600 °C, hence the higher initiation of activation occurs at a higher temperature for the K_2CO_3 system. The melting point of K_2CO_3 is too high (ca 890 °C) to permit the formation of a bulk molten phase (as observed for KOH activation) and the majority of the K_2CO_3 remains inactive during the lower temperature (<600 °C) activation.

For a given degree of burn-off, K_2CO_3 produced carbons with a lower micropore volume and a more heterogenous pore size distribution than KOH. The higher temperatures required for K_2CO_3 activation produce less reaction of the alkali with the char. Also, the contribution of the physical gasification reactions was much greater, due to the production of significant quantities of CO_2.

Activation with KOH allows extensive creation of micropores at low temperatures, prior to the onset of pore widening and surface erosion at high temperatures. In contrast, pore creation and pore widening/surface erosion are occurring simultaneously in the K_2CO_3 system, leading to less efficient creation of pores and a wider pore size distribution.

CRediT authorship contribution statement

James M. Illingworth: Investigation, Writing – original draft. **Brian Rand:** Supervision. **Paul T. Williams:** Supervision, Writing – review & editing, Funding acquisition.

Declaration of Competing Interest

The authors declare that they have no known competing financial interests or personal relationships that could have appeared to influence the work reported in this paper.

Acknowledgements

A scholarship from the UK Engineering & Physical Sciences Research Council (EPSRC) is gratefully acknowledged for one of us (JMI).

References

[1] M.A. Yahya, Z. Al-Qodah, C.C.Z. Ngah, Agricultural bio-waste materials as potential sustainable precursors used for activated carbon production: a review, Renew. Sust. Energ. Rev. 46 (2015) 218–235.
[2] K.S. Ukanwa, K. Patchigolla, R. Sakrabani, E. Anthony, S. Mandavgane, A review of chemicals to produce activated carbon from agricultural waste biomass, Sustainability 11 (2019). Article #6206.
[3] E. Koseoilu, C. Akmil-Basar, Preparation, structural evaluation and adsorptive properties of activated carbon from agricultural waste biomass, Adv. Powder Technol. 26 (2015) 811–818.
[4] B. Zhang, Y.Q. Jiang, R. Balasubramanian, Synthesis, formation mechanisms and applications of biomass-derived carbonaceous materials: a critical review, J. Mater. Chem. A 9 (44) (2021) 24759–24802.
[5] M. Gayathiri, T. Pulingam, K.T. Lee, K. Sudesh, Activated carbon from biomass waste precursors: Factors affecting production and adsorption mechanism, Chemosphere 294 (2022). Article #133764.
[6] B. Docekalska, M. Bartkowiak, H. Lopatka, M. Zborowska, Activated carbon prepared from corn biomass by chemical activation with potassium hydroxide, Bioresources 17 (1) (2022) 1794–1804.
[7] M.A. Nahil, P.T. Williams, Characterisation of activated carbons with high surface area and variable porosity produced from agricultural cotton waste by chemical activation and co-activation, Waste Biomass Valoris. 3 (2012) 117–130.
[8] T. Alfatah, E.M. Mistar, M.D. Supardan, Porous structure and adsorptive properties of activated carbon derived from Bambusa vulgaris striata by two-stage KOH/NaOH mixture activation for Hg2+ removal. Journal of Water, Process. Eng. 43 (2021). Article #102294.
[9] M.J. Ahmed, Preparation of activated carbons from date (phoenix dactylifera L.) palm stones and application for waste water treatments: a review, Process. Saf. Environ. Prot. 102 (2016) 168–182.
[10] N. Arena, J. Lee, R. Clift, Life cycle assessment of activated carbon production from coconut shells, J. Clean. Prod. 125 (2016) 68–77.
[11] Y. Ma, Comparison of activated carbons prepared from wheat straw via $ZNCl_2$ and KOH activation, Waste Biomass Valoriz. 8 (2017) 549–559.
[12] C.N. Wang, L.J. Bai, F. Zhao, L.Z. Bai, Activated carbon fibers from cattail fibers for supercapacitors, Carbon Lett. 32 (2022) 907–915.
[13] X. Zhang, Z. Li, X. Tian, Y. Ma, L. Ma, Highly ordered microporous activated carbon from long fiber biomass for high energy density supercapacitors, Chem. Select 6 (45) (2021) 13015–13023.
[14] H.M. Nasir, S.Y. Wee, A.Z. Aris, L.C. Abdullah, I. Ismail, Processing of natural fibre and method improvement for removal of endocrine-disrupting compounds, Chemosphere 291 (1) (2022). Article #132726.
[15] Y. Zhao, Q.Z. Lua, V. Guna, N. Reddy, Natural cellulose fibers from stems of Chrysanthemum Indicum, J. Nat. Fibers (2021) 1–12, https://doi.org/10.1080/15440478.2021.1982823. Article #1982823.
[16] K.J. Hwang, J.Y. Park, Y.J. Kim, G. Kim, C. Choi, S. Jin, N. Kim, J.W. Lee, W. G. Shim, Adsorption behaviour on hollow activated carbon fibre from biomass, Sep. Sci. Technol. 50 (12) (2015) 1757–1767.
[17] J.M. Illingworth, B. Rand, P.T. Williams, Non-woven fabric activated carbon production from fibrous waste biomass for Sulphur dioxide control, Process. Saf. Environ. Prot. 122 (2019) 209–220.
[18] M.F. Hassan, M.A. Sabri, H. Fazal, A. Hafeez, N. Shezad, M. Hussain, Recent trends in activated carbon fibers production from various precursors and applications- a comparative review, J. Anal. Appl. Pyrolysis 145 (2020). Article #104715.
[19] P.T. Williams, A.R. Reed, Pre-formed activated carbon matting derived from the pyrolysis of biomass natural fibre textile waste, J. Anal. Appl. Pyrolysis 70 (2003) 563–577.
[20] P.T. Williams, A.R. Reed, 'High grade activated carbon matting derived from the chemical activation and pyrolysis of natural fibre textile waste', J. Anal. Appl. Pyrolysis 71 (2004) 971–986.
[21] P.T. Williams, A.R. Reed, Development of activated carbon pore structure via physical and chemical activation of biomass fibre waste, Biomass Bioenergy 30 (2006) 144–152.

[22] M. Kwiatkowski, E. Broniek, Computer analysis of the porous structure of activated carbons derived from various biomass materials by chemical activation, Materials 14 (2021). Article #4121.
[23] J. Bolton, The potential of plant fibres as crops for industrial use, Outl. Agric. 24 (2) (1995) 85–89.
[24] Y. Yamashita, K. Ouchi, Influence of alkali on the carbonization process – III, Carbon 20 (1) (1982) 55–61.
[25] T. Otowa, M. Yamada, R. Tanibata, M. Kawakami, Preparation, pore analysis and adsorption behaviour of high surface area active carbon from coconut shell, in: E. F. Vansant, R. Dewolfs (Eds.), Gas Separation Technology, Elsevier, Amsterdam, 1990.
[26] A. Ahmadpour, D.D. Do, The preparation of active carbons from coal by chemical and physical activation, Carbon 34 (4) (1996) 471–479.
[27] H.S. Teng, Li-Yeh Hsu, High porosity carbons prepared from bituminous coal with potassium hydroxide activation, Ind. Eng. Chem. Res. 38 (1999) 2947–2953.
[28] M.J.B. Evans, E. Halliop, J.A.F. MacDonald, The production of chemically-activated carbon, Carbon 37 (2) (1999) 269–274.
[29] J. Hayashi, A. Kazehaya, K. Muroyama, A.P. Watkinson, Preparation of activated carbons from lignin by chemical activation, Carbon 38 (13) (2000) 1873–1878.
[30] K. Okada, N. Yamamoto, Y. Kameshina, A. Yasumori, Porous properties of activated carbons from waste newspaper prepared by chemical and physical activation, J. Colloid Interface Sci. 262 (1) (2003) 179–193.
[31] T. Yang, A.C. Lua, Characteristics of activated carbons prepared from pistachio-nut shells by potassium hydroxide activation, Microporous Mesoporous Mater. 63 (2003) 113–124.
[32] R.P. Bansal, J.B. Donnet, F. Stoeckli, Active Carbon, Marcel Dekker, New York, 1988.
[33] H. Benaddi, D. Legras, J.N. Rouzaud, F. Beguin, Influence of the atmosphere in the chemical activation of wood by phosphoric acid, Carbon 36 (3) (1998) 306–309.
[34] R.D. Harrison (Ed.), Nuffield Advanced Science Book of Data, Longman Group, London, 1977.
[35] X. Chen, B. McEnaney, Activation of meso-carbon microbeads with KOH, in: Carbon 2001 Extended Abstracts, Lexington, Kentucky, USA, 2001.
[36] M.A. Lillo-Rodenas, D. Cazorla-Amoros, A. Linares-Solano, Understanding reactions between carbons and NaOH and KOH: an insight into the chemical activation mechanism, Carbon 41 (2) (2003) 267–275.
[37] Y. Yamashita, K. Ouchi, Influence of alkali on the carbonization process – I, Carbon 20 (1) (1982) 41–45.
[38] M.J. Denial, L. Davies, A.W. Locke, M.E. Reay, Investigating Chemistry, Heinemann Educational, London, 1982.
[39] P. Matthews, Advanced Chemistry, in: Volume 1: Physical and Industrial, Cambridge University Press, Cambridge, 1992.
[40] P. Matthews, Advanced Chemistry, in: Volume 2: Organic and Inorganic, Cambridge University Press, Cambridge, 1992.
[41] Y. Yamashita, K. Ouchi, Influence of alkali on the carbonization process – II, Carbon 20 (1) (1982) 47–53.
[42] C. Mims, J.K. Pabst, Role of surface salt complexes in alkali catalysed carbon gasification, Fuel 62 (2) (1983) 176–179.